Contrib Mineral Petrol (2011) 162:231–252
DOI 10.1007/s00410-010-0592-1

ORIGINAL PAPER

Geochemistry of southern Pagan Island lavas, Mariana arc: the role of subduction zone processes

Jared P. Marske · Aaron J. Pietruszka · Frank A. Trusdell · Michael O. Garcia

Received: 23 November 2009 / Accepted: 3 November 2010 / Published online: 19 November 2010

Abstract New major and trace element abundances, and Pb, Sr, and Nd isotopic ratios of Quaternary lavas from two adjacent volcanoes (South Pagan and the Central Volcanic Region, or CVR) located on Pagan Island allow us to investigate the mantle source (i.e., slab components) and melting dynamics within the Mariana intra-oceanic arc. Geologic mapping reveals a pre-caldera (780–9.4 ka) and post-caldera (<9.4 ka) eruptive stage for South Pagan, whereas the eruptive history of the older CVR is poorly constrained. Crystal fractionation and magma mixing were important crustal processes for lavas from both volcanoes. Geochemical and isotopic variations indicate that South Pagan and CVR lavas, and lavas from the northern volcano on the island, Mt. Pagan, originated from compositionally distinct parental magmas due to variations in slab contributions (sediment and aqueous fluid) to the mantle wedge and the extent of mantle partial melting. A mixing model based on Pb and Nd isotopic ratios suggests that the average amount of sediment in the source of CVR (~2.1%) and South Pagan (~1.8%) lavas is slightly higher than Mt. Pagan (~1.4%) lavas. These estimates span the range of sediment-poor Guguan (~1.3%) and sediment-rich Agrigan (~2.0%) lavas for the Mariana arc. Melt modeling demonstrates that the saucer-shaped normalized rare earth element (REE) patterns observed in Pagan lavas can arise from partial melting of a mixed source of depleted mantle and enriched sediment, and do not require amphibole interaction or fractionation to depress the middle REE abundances of the lavas. The modeled degree of mantle partial melting for Agrigan (2–5%), Pagan (3–7%), and Guguan (9–15%) lavas correlates with indicators of fluid addition (e.g., Ba/Th). This relationship suggests that the fluid flux to the mantle wedge is the dominant control on the extent of partial melting beneath Mariana arc volcanoes. A decrease in the amount of fluid addition (lower Ba/Th) and extent of melting (higher Sm/Yb), and an increase in the sediment contribution (higher Th/Nb, La/Sm, and Pb isotopic ratios) from Mt. Pagan to South Pagan could reflect systematic cross-arc or irregular along-arc melting variations. These observations indicate that the length scale of compositional heterogeneity in the mantle wedge beneath Mariana arc volcanoes is small (~10 km).

Keywords Subduction · Partial melting · Mariana arc · Pagan Island · Volcanoes

Communicated by T. L. Grove.

Electronic supplementary material The online version of this article (doi:10.1007/s00410-010-0592-1) contains supplementary material, which is available to authorized users.

J. P. Marske (✉) · M. O. Garcia
Department of Geology and Geophysics, University of Hawaii, Honolulu, HI 96822, USA
e-mail: marske@hawaii.edu

A. J. Pietruszka
Department of Geological Sciences, San Diego State University, San Diego, CA 92182, USA

F. A. Trusdell
Hawaii Volcano Observatory, United States Geological Survey, Hawaii Volcanoes National Park, Hawaii, HI 96718, USA

Introduction

Magma generation at subduction zones is one of the most important yet enigmatic geologic processes on Earth.

Subduction zone magmatism involves the transfer of chemical components from the subducted slab into the mantle wedge, a process that modifies the mantle composition and triggers melting (e.g., Gill 1981). Two main slab-derived components, commonly characterized as sediment or sediment melts and aqueous fluids, are invoked to explain much of the compositional variation in arc lavas (e.g., Elliott et al. 1997; Plank and Langmuir 1998; Stern et al. 2003; Tollstrup and Gill 2005; Shaw et al. 2008). Arc magmas generated at continental convergent margins can be further modified by crustal assimilation (e.g., Andean, Stern and Kilian 1996; Alaska-Aleutian, George et al. 2003; Cascade, Jicha et al. 2009), obscuring the slab-related geochemical signatures in the lavas. In contrast, intra-oceanic convergent margins (i.e., Izu-Bonin-Mariana arcs) are ideal locations to study the processes that operate within the mantle wedge because the compositional effects of crustal contamination are likely minimal compared to continental convergent margins (Elliott et al. 1997).

Geochemical studies of individual or closely spaced arc volcanoes over relatively short time periods (e.g., hundreds to tens of thousands of years) provide valuable insight into the fine-scale changes in mantle source composition and melting conditions related to variable fluxes of sediment (melts) and aqueous fluids to the mantle wedge (e.g., Dungan et al. 2001; Yokoyama et al. 2003; Bolge et al. 2006). Mariana intra-oceanic arc lavas have been well studied. Previous whole-rock and melt inclusion studies have identified the fluid-rich (Guguan Volcano) and sediment-rich (Agrigan Volcano) end members for Mariana arc lavas (Elliott et al. 1997; Tollstrup and Gill 2005), although no clear systematic along-arc geochemical variations have been recognized. Instead, the compositional differences are thought to reflect varying proportions of aqueous fluid and sediment contributions to individual melting regions beneath these volcanoes (Kent and Elliott 2002).

Here we present a comprehensive geochemical study of lavas from two adjacent volcanoes on Pagan Island, South Pagan and the Central Volcanic Region (CVR). Pagan Island is one of the most active volcanic centers in the Mariana arc (Fig. 1) and is located between Agrigan and Guguan. Stratigraphically controlled Quaternary to Holocene lavas from South Pagan and the CVR were collected and analyzed for major- and trace element abundances and Pb, Sr, and Nd isotopic ratios to investigate small-scale spatial and temporal compositional variations between these adjacent volcanoes. The primary goals of this paper are to identify the slab contributions (fluid and sediment components) to the subarc mantle and evaluate the nature and extent of mantle partial melting beneath Mariana arc volcanoes. These results will help to elucidate the nature of subduction zone processes at Pagan Island, one of the least studied volcanic centers in the Mariana arc.

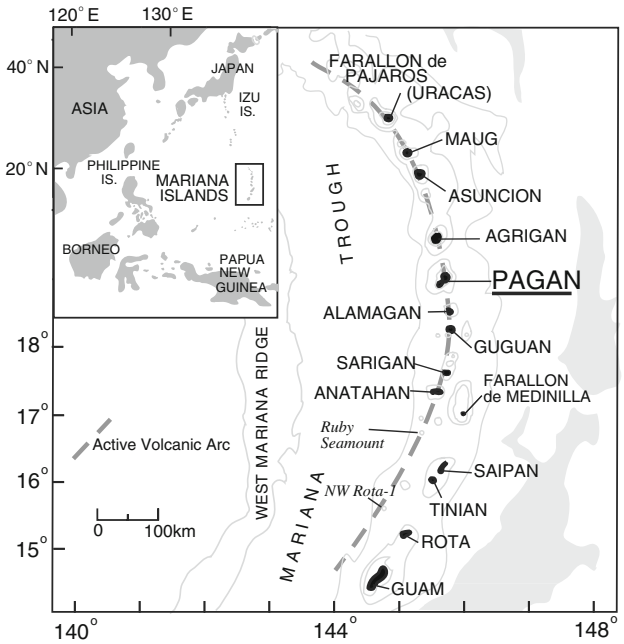

Fig. 1 Location map of the Northern Mariana Islands modified from Karig (1971). The nine islands extending from Anatahan to Farallon de Parajos delineate the active subaerial volcanic arc. The *inset map* shows the regional location of the Northern Mariana Islands in the western Pacific Ocean. The *shaded gray areas* to the right of the active arc denote the location of the Mariana trench. Ocean Drilling Project Site 801 is located ~900 km east of the Mariana trench at 18° 38.538′N 156° 21.588′E

Pagan geology and sampling

Pagan has the largest subaerial surface area (~65 km^2; Trusdell 2009) and volume (2,160 km^3; Bloomer et al. 1989a) among the active Mariana volcanic islands (Fig. 1). The island consists of two stratovolcanoes, South Pagan (548 m) and Mt. Pagan (570 m) that are joined by the CVR, an eroded remnant of several extinct Quaternary stratovolcanoes (Trusdell 2009). The CVR is a 4-km-long, 70–580 m high ridge consisting of steeply to moderately dipping, 0.3–10 m thick basaltic a'a lavas interbedded with rare pyroclastic deposits. The CVR is older than both Mt. Pagan and South Pagan based on stratigraphic relationships and the deeply eroded nature of the volcanic edifice (Trusdell 2009). Mount Pagan and South Pagan have Holocene cones within their 6- and 4-km-wide Quaternary calderas, respectively (Corwin et al. 1957; Trusdell et al. 2006). Lavas from these two volcanoes were subdivided into two main eruptive periods termed the pre- and post-caldera stages (Fig. 2), which are defined as having erupted before or after the formation of their respective calderas.

South Pagan has three intra-caldera Holocene cones (Bulikan Bulifli, Seismic, and Bilikan Paliat) with 100–150-m-deep summit craters (Trusdell 2009; Fig. 2). Bulikan Bulifli is a broad, low-lying cone that produced the

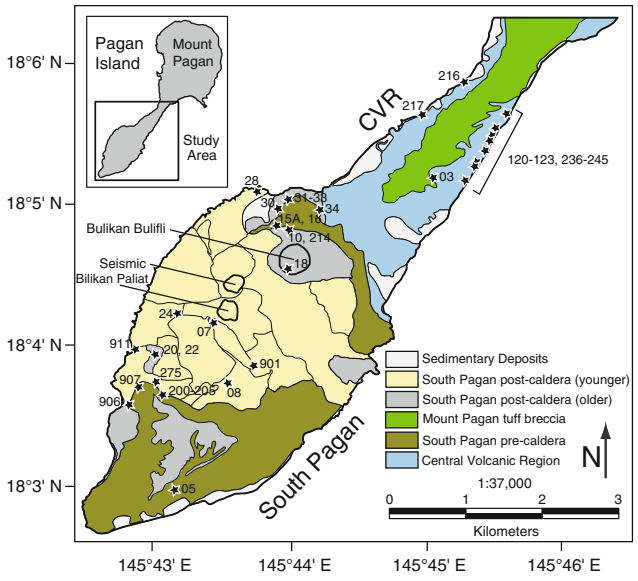

Fig. 2 Simplified geologic map of southern Pagan Island showing the distribution of CVR lavas, and South Pagan pre- and post-caldera stage lavas, the Mt. Pagan tuff breccia unit, and sedimentary deposits. South Pagan post-caldera units are divided into older and younger groups based on stratigraphy. The *thin lines* within the South Pagan post-caldera (younger) unit delineate individual lava flows and tephra deposits. Sample locations are plotted and are listed in Table A1—Electronic Supplementary Material. Locations for samples TM-06-15A, TM-06-16, and TM-06-34 are approximate. South Pagan post-caldera cones are outlined in *black*

oldest exposed post-caldera flows that surface the northeast floor of the caldera. The most recent post-caldera flows cover most of the western flank and floor of the caldera. They originated from the Seismic and Bilikan Paliat cones, which are coalesced along a NE-SW axis (Fig. 2). South Pagan's historical eruptive record is relatively short and intermittently recorded. The only verified historical South Pagan eruption occurred in 1864 A.D., although the volcano may have erupted in 1929 A.D. (Simkin et al. 1981). New carbon-14 dating of charcoal beneath a post-caldera tephra (not analyzed in this study) yielded an age of 670 ± 50 years BP (F. Trusdell, unpublished data, 2010). The youngest stratigraphically controlled South Pagan post-caldera samples (TM-06-275 and TM-06-911; collected from the same lava flow 500 m apart) underlie the 670 ± 50 years BP tephra.

Mount Pagan has a single symmetrical cone and two maar basins within its ~9.4-ka caldera (Trusdell et al. 2006). A prominent deposit ("Mount Pagan tuff breccia"; Fig. 2), thought to have been produced during the formation of Mt. Pagan caldera (Trusdell et al. 2006), caps much of the CVR (Fig. 2). Lavas at the base of the inner caldera wall of Mt. Pagan are <780 kyr old based on the observation that they are normally magnetized (Larson et al. 1974). Mount Pagan is the most historically active Mariana volcano with 15 eruptions in ~350 years (Simkin et al. 1981; Trusdell 2009). Its most explosive historical eruption (VEI = 4) in May 1981 produced a sub-plinian column followed by basaltic a'a flows and air-fall deposits totaling ~0.2 km^3 (Banks et al. 1984).

Forty-two samples (37 flows and 5 dikes) that encompass a wide geographical and temporal range for South Pagan and the CVR were analyzed. A majority of these lavas were sampled stratigraphically along the steeply eroded east side of the CVR, and on the flanks, inner walls, and floor of South Pagan caldera (Fig. 2). Most CVR lavas are thought to be significantly older than South Pagan pre-caldera lavas based on new $^{40}Ar/^{39}Ar$ dating (Table A1—Electronic Supplementary Material). A CVR lava (TM-06-238) collected near the base of the subaerially exposed CVR section (Fig. 2) yielded an age of 286 ± 56 kyr, whereas the oldest stratigraphically controlled pre-caldera lava collected from the lower western flank of South Pagan (not analyzed in this study) was dated at 64 ± 15 kyr (F. Trusdell, unpublished data, 2010). A South Pagan pre-caldera lava collected from the upper part of the southern caldera wall (TM-06-205) is significantly younger (12 ± 15 ka) than both of the other dated samples (Table A1—Electronic Supplementary Material; Fig. 2). The two youngest CVR flows sampled (TM-06-03 and TM-06-34), termed "late-stage CVR" (Table 1), are probably closer in age to the oldest South Pagan pre-caldera lavas rather than the 286 ± 56 ka lava from the subaerially exposed CVR section (Fig. 2) based on stratigraphic relationships. Sample TM-06-34 is overlain by South Pagan pre-caldera flows at the base of the northern flank of the South Pagan caldera, whereas sample TM-06-03 is a flow located near the top of the CVR that directly underlies the ~9.4-ka Mt. Pagan tuff breccia (Fig. 2).

Relative stratigraphic order for four suites of lavas from the CVR and South Pagan was determined by geologic mapping (Table 1; Fig. 2). In order from oldest to youngest, these suites are (1) Ten lavas sampled from an ~830 m section along the east coast of the CVR. These lavas were sampled ~300 vertical meters below the Mt. Pagan tuff breccia unit. (2) A late-stage CVR lava (TM-06-03) that predates South Pagan pre-caldera lavas. (3) Nine South Pagan pre-caldera lavas from a ~175 m section along the volcano's southwest flank and wall. (4) Five South Pagan post-caldera lavas originating from the Holocene cones that surface the caldera floor. In addition, five dikes (three from the CVR and two from South Pagan) were analyzed. The ages of the dikes are unknown, but the observation that they crosscut CVR and South Pagan pre-caldera lavas suggests they likely predate South Pagan post-caldera lavas. For the purposes of plotting and discussion, the CVR and South Pagan dikes are considered to

Table 1 Whole-rock XRF analyses of southern Pagan lavas

Sample	Strat #	SiO_2	TiO_2	Al_2O_3	FeO*	MnO	MgO	CaO	Na_2O	K_2O	P_2O_5	Total
South Pagan post-caldera												
TM-06-15A	–	52.05	0.79	17.00	9.23	0.18	5.50	10.79	2.29	0.82	0.14	98.79
TM-06-16	–	61.76	0.73	15.44	6.79	0.17	1.97	4.84	3.92	2.16	0.22	98.00
TM-06-10	–	53.50	0.81	17.08	9.04	0.18	4.93	10.08	2.79	1.01	0.16	99.58
TM-06-10r	–	53.49	0.81	17.08	9.16	0.18	4.93	10.08	2.80	1.01	0.16	99.70
TM-06-901	–	53.86	0.81	17.08	9.04	0.18	4.80	9.97	2.82	1.08	0.16	99.79
TM-06-28	–	53.83	0.80	16.88	9.13	0.18	4.83	9.90	2.80	1.09	0.16	99.60
TM-06-08	–	53.89	0.79	16.79	9.08	0.18	4.92	9.94	2.75	1.10	0.16	99.60
TM-06-07	–	52.48	0.78	17.23	9.25	0.18	4.92	9.90	2.62	0.97	0.15	98.49
TM-06-275	24	53.88	0.78	16.73	9.10	0.18	4.96	10.06	2.73	1.09	0.16	99.66
TM-06-911	24	53.98	0.79	16.95	9.10	0.18	4.92	10.10	2.77	1.10	0.15	100.04
TM-06-214	23	53.60	0.80	16.76	9.32	0.18	4.89	10.00	2.76	1.07	0.16	99.54
TM-06-24	22	52.68	0.79	17.19	9.17	0.18	5.15	10.47	2.61	0.91	0.14	99.29
TM-06-18	21	60.12	0.79	16.03	6.85	0.16	2.25	5.82	3.85	1.93	0.23	98.04
South Pagan dikes												
TM-06-20	–	52.27	0.79	17.17	9.18	0.18	5.33	10.49	2.61	0.86	0.15	99.03
TM-06-22	–	52.20	0.84	17.64	9.40	0.18	4.82	10.34	2.76	0.87	0.16	99.20
South Pagan pre-caldera												
TM-06-30	–	61.21	0.91	15.60	7.49	0.18	1.99	5.15	4.23	2.08	0.31	99.15
TM-06-30r	–	61.18	0.90	15.61	7.42	0.18	1.99	5.16	4.23	2.08	0.31	99.06
TM-06-31	–	52.28	0.78	16.98	9.39	0.18	5.60	10.89	2.47	0.90	0.14	99.60
TM-06-32	–	54.33	0.76	16.87	8.90	0.18	4.75	9.58	2.84	1.12	0.16	99.49
TM-06-33	–	55.09	0.79	17.02	8.82	0.18	4.27	8.86	3.06	1.23	0.18	99.49
TM-06-05	20	54.71	0.87	18.26	8.42	0.17	3.23	8.81	3.15	1.14	0.18	98.93
TM-06-205	19	53.28	0.77	17.39	8.83	0.18	5.24	10.65	2.66	0.87	0.13	100.00
TM-06-204	18	53.17	0.76	17.51	8.85	0.17	5.12	10.60	2.51	0.87	0.13	99.69
TM-06-203	17	52.85	0.76	17.38	8.90	0.18	5.19	10.43	2.67	0.85	0.13	99.34
TM-06-202	16	52.97	0.77	17.36	8.93	0.18	5.22	10.57	2.49	0.84	0.12	99.44
TM-06-201	15	52.46	0.78	17.24	9.10	0.18	5.15	10.28	2.65	0.86	0.12	98.81
TM-06-200	14	52.70	0.77	17.21	8.89	0.18	5.07	10.28	2.61	0.89	0.13	98.72
TM-06-907	13	61.60	0.70	16.62	6.07	0.15	2.04	5.54	4.46	1.62	0.21	99.01
TM-06-906	12	57.56	0.86	16.27	8.75	0.19	3.26	7.12	3.61	1.60	0.23	99.45
CVR dikes												
TM-06-241	–	50.42	0.76	19.27	9.06	0.18	4.80	11.71	2.59	0.58	0.11	99.49
TM-06-217	–	48.25	0.77	19.31	10.15	0.19	5.66	13.22	2.08	0.46	0.10	100.18
TM-06-120	–	48.99	0.80	17.86	10.90	0.21	5.64	11.92	2.43	0.63	0.13	99.51
Late-stage CVR												
TM-06-03	11	56.15	0.74	18.26	7.69	0.17	2.89	8.19	3.67	1.18	0.16	99.10
TM-06-34	–	52.41	0.81	18.93	8.91	0.17	3.73	10.37	2.83	0.87	0.15	99.17
Central Volcanic Region												
TM-06-216	10	49.48	0.80	17.21	10.78	0.21	6.28	11.89	2.31	0.56	0.13	99.66
TM-06-236	9	48.63	0.83	17.92	11.32	0.21	5.55	12.04	2.35	0.59	0.15	99.58
TM-06-237	8	48.93	0.80	17.50	11.08	0.21	5.87	12.13	2.33	0.60	0.13	99.60
TM-06-123	7	48.38	0.80	17.58	11.07	0.21	5.88	12.06	2.30	0.55	0.13	98.98
TM-06-122	6	49.11	0.79	17.72	10.98	0.21	5.89	12.02	2.26	0.63	0.13	99.73
TM-06-121	5	49.24	0.79	18.39	10.88	0.21	5.51	11.81	2.40	0.61	0.14	99.97
TM-06-238	4	49.56	0.77	18.65	10.65	0.20	5.31	11.76	2.42	0.64	0.14	100.09
TM-06-239	3	49.16	0.74	17.76	10.61	0.20	5.95	12.12	2.24	0.57	0.13	99.48

Table 1 continued

Sample	Strat #	SiO_2	TiO_2	Al_2O_3	FeO*	MnO	MgO	CaO	Na_2O	K_2O	P_2O_5	Total
TM-06-245	2	49.18	0.76	18.53	10.61	0.20	5.39	11.75	2.36	0.61	0.13	99.52
TM-06-243	1	51.58	0.72	16.78	9.54	0.18	5.66	10.81	2.58	0.86	0.14	98.85
Hawaiian Rock Standard												
Kil1919[a]	–	50.26	2.83	13.83	11.08	0.17	7.15	11.65	2.32	0.53	0.27	100.1
Kil1919[b]	–	50.61	2.80	13.91	11.01	0.18	6.96	11.56	1.80	0.54	0.28	99.65

Sample	LOI	Y	Sr	Rb	Zr	Ni	Cr	V	Ba
South Pagan post-caldera									
TM-06-15A	0.85	21.9	322	15.1	78	21	32	268	186
TM-06-16	1.12	38.0	277	41.2	172	b.d.	b.d.	111	391
TM-06-10	−0.13	23.2	317	18.5	85	13	25	269	197
TM-06-10r	−0.13	23.0	316	18.5	86	12	25	269	204
TM-06-901	−0.10	23.9	316	19.8	89	12	21	269	201
TM-06-28	−0.02	24.4	308	20.0	90	11	16	269	201
TM-06-08	−0.09	24.5	302	20.1	91	12	20	268	203
TM-06-07	0.99	22.7	303	17.8	87	12	20	267	200
TM-06-275	−0.04	24.4	303	20.3	90	13	22	269	208
TM-06-911	−0.23	24.4	307	20.2	89	13	22	271	202
TM-06-214	−0.13	24.0	306	19.3	88	12	15	271	201
TM-06-24	0.09	22.7	317	17.1	78	13	26	271	186
TM-06-18	0.83	34.6	286	36.7	158	b.d.	3	148	358
South Pagan dikes									
TM-06-20	0.32	22.1	341	14.5	71	19	39	279	176
TM-06-22	0.27	22.8	351	14.9	72	15	23	295	186
South Pagan pre-caldera									
TM-06-30	−0.09	41.5	322	36.7	161	b.d.	b.d.	114	418
TM-06-30r	−0.09	40.0	321	38.0	163	b.d.	b.d.	116	417
TM-06-31	−0.04	21.4	321	16.9	77	21	37	272	177
TM-06-32	0.03	23.7	378	18.6	87	16	20	265	247
TM-06-33	−0.11	26.4	377	20.9	97	14	15	255	260
TM-06-05	0.37	26.6	341	21.5	98	4	8	246	226
TM-06-205	−0.19	22.0	330	15.4	76	18	50	273	187
TM-06-204	−0.14	21.8	333	14.5	76	18	47	270	186
TM-06-203	0.20	21.3	328	15.2	75	19	48	254	193
TM-06-202	0.15	22.4	330	14.1	75	19	48	273	187
TM-06-201	0.72	21.1	325	14.7	76	18	46	251	192
TM-06-200	0.65	22.4	326	15.3	75	17	44	266	195
TM-06-907	0.17	34.8	326	26.8	127	b.d.	3	131	349
TM-06-906	0.17	31.2	298	28.9	128	5	17	197	291
CVR dikes									
TM-06-241	−0.15	17.8	379	9.8	50	16	19	298	129
TM-06-217	−0.32	13.4	387	7.5	32	11	17	353	101
TM-06-120	−0.23	18.2	447	8.9	43	16	17	345	156
Late-stage CVR									
TM-06-03	−0.02	26.1	365	19.0	92	3	3	213	244
TM-06-34	0.19	22.6	388	14.2	71	6	10	281	185
Central Volcanic Region									
TM-06-216	−0.09	20.2	400	8.1	41	16	19	324	143

Table 1 continued

Sample	LOI	Y	Sr	Rb	Zr	Ni	Cr	V	Ba
TM-06-236	−0.22	18.8	453	7.4	40	14	8	362	153
TM-06-237	−0.30	18.2	436	7.0	41	17	17	351	145
TM-06-123	−0.03	17.9	442	6.7	43	17	14	342	151
TM-06-122	−0.04	17.5	445	9.5	40	18	18	339	155
TM-06-121	−0.08	18.1	469	7.7	40	17	25	333	160
TM-06-238	−0.15	17.2	476	8.7	39	18	28	327	158
TM-06-239	0.04	17.2	448	8.3	39	24	54	328	153
TM-06-245	−0.16	17.0	473	7.4	40	18	26	337	156
TM-06-243	0.28	19.4	395	14.3	59	20	49	302	192
Hawaiian Rock Standard									
Kil1919[a]	−0.48	27.0	405	9.3	176	103	261	320	136
Kil1919[b]	–	24.7	395	9.0	177	101	266	284	124

Total iron is given as FeO*. Oxide abundances are in wt. %; trace element contents are in ppm. Loss on ignition (LOI) values are in %. Negative LOI values indicate gain on ignition. Relative stratigraphic position (Strat #) is known for some lavas. Older to younger lavas correspond to increasing values (1–24). Replicate analyses (*r*) are given for TM-06-10 and TM-06-30

[a] The Hawaiian in-house rock standard Kil1919 ($n = 1$), analyzed with the Pagan samples, was collected from the same lava flow as the BHVO-1 and -2 standards

[b] Reference standard values for Kil1919 are from Rhodes and Vollinger (2004). Element concentrations below the detection limit are noted as "b.d.". Sample locations are presented in Table A1—Electronic Supplementary Material

be part of the CVR and South Pagan pre-caldera stages, respectively.

Analytical methods

Major and trace element (Rb, Sr, Y, Zr, Ni, Cr, V, and Ba) abundances for 42 samples (Table 1) were determined using X-ray fluorescence spectrometry (XRF) at Washington State University (WSU) using methods described by Johnson et al. (1999). Prior to the XRF analysis, the samples were crushed between tungsten carbide plates, ultrasonically washed three times in deionized water for 2–4 min, and hand-picked under a binocular microscope to avoid chips with any signs of alteration. The selected chips (~35 g) were then powdered using a tungsten carbide swing mill. Estimates of analytical precision for XRF major and trace element abundances are based on duplicate analyses of samples TM-06-10 and TM-06-30, which agree to within 2% for all elements (Table 1). All estimates of precision in this paper are given as $\pm 2\sigma$ (except for the XRF data, which is based on the % difference of the replicate analyses). A Hawaiian basaltic rock in-house standard (Kil1919, $n = 1$) was analyzed with the samples to evaluate the accuracy of the XRF data. Comparison XRF Kil1919 values ($n = 6$) from Rhodes and Vollinger (2004) show that all element abundances agree within 4% except for MnO (6%), Ba (9%), Y (9%), V (11%), and Na_2O (23%).

Fifteen samples were analyzed for Sc, Cs, Rb, Ba, Sr, Th, U, Pb, Nb, Ta, Hf, Zr, Y, and REE abundances using inductively coupled plasma mass spectrometry (ICP-MS) at WSU (Table 2). The samples were prepared as described for the XRF analyses, but were powdered using an agate mortar and pestle. Analytical methods for the ICP-MS analyses are described in Knaack et al. (1994). Estimates of analytical precision are based on the TEB in-house standard because it has trace element concentrations similar to the Pagan samples. Replicate analyses of the TEB standard ($n = 54$) analyzed over a 3-year period show that all elements agree within 5% except for Sc (8%), Nb (9%), Ta (12%), U (13%), Pb (15%), Rb (16%), Th (16%), and Cs (17%). These are considered maximum estimates for this study because the Pagan samples were analyzed in a single session. The Kil1919 ($n = 2$) in-house standard (analyzed with the samples) agrees with comparison ICP-MS Kil1919 values ($n = 11$) from Pietruszka and Garcia (1999) within 2% for all elements (Table 2) except for Dy (3%), Nb (3%), and Hf (13%). The trace element abundances determined by both XRF and ICP-MS agree within 10% for all samples except for six that agree within 15%. No interlaboratory bias corrections were made to Mariana literature trace element data discussed in this paper due to the absence of common rock standards.

Fifteen South Pagan and CVR lavas were analyzed from hand-picked rock chips for Pb, Sr, and Nd isotopic ratios (Table 3) at San Diego State University (SDSU) using the chemical and mass spectrometric procedures described in Marske et al. (2007). Isotopic ratios of Pb and Nd were measured with a Nu Plasma HR multi-collector inductively coupled plasma mass spectrometer

Table 2 ICP-MS trace element analyses of southern Pagan lavas

Sample	Rb	Cs	Ba	La	Ce	Pr	Nd	Sm	Eu	Gd	Tb	Dy	Ho	Er
South Pagan post-caldera														
TM-06-275	21.9	0.660	217	8.07	17.6	2.61	12.0	3.41	1.02	3.97	0.69	4.34	0.92	2.59
TM-06-214	22.3	0.645	216	8.05	17.6	2.62	12.0	3.39	1.05	4.05	0.69	4.38	0.93	2.59
TM-06-24	19.4	0.570	198	7.56	16.4	2.46	11.2	3.20	1.03	3.75	0.65	4.06	0.88	2.45
TM-06-18	38.5	1.16	373	14.0	30.1	4.36	19.5	5.24	1.39	5.96	1.02	6.47	1.37	3.91
South Pagan pre-caldera														
TM-06-05	22.7	0.688	238	9.10	20.0	2.98	13.8	3.85	1.19	4.54	0.78	4.96	1.05	2.95
TM-06-202	15.3	0.361	202	7.47	16.1	2.38	11.1	3.15	0.99	3.69	0.63	4.05	0.85	2.42
CVR Dike														
TM-06-217	8.1	0.180	100	4.27	9.18	1.44	6.93	2.12	0.83	2.60	0.44	2.80	0.57	1.61
Late-Stage CVR														
TM-06-03	20.7	0.305	252	9.17	19.6	2.92	13.3	3.70	1.20	4.30	0.75	4.74	1.01	2.86
TM-06-34	15.3	0.416	196	7.40	15.7	2.41	11.1	3.20	1.08	3.78	0.64	4.11	0.86	2.46
Central Volcanic Region														
TM-06-216	9.1	0.221	149	5.87	12.9	1.95	9.50	2.86	1.02	3.41	0.58	3.70	0.77	2.17
TM-06-236	7.5	0.124	147	6.14	13.0	1.96	9.38	2.71	0.98	3.15	0.53	3.34	0.70	1.97
TM-06-237	7.7	0.151	151	5.91	12.8	1.93	9.28	2.73	0.97	3.23	0.55	3.48	0.73	2.05
TM-06-239	9.3	0.258	167	6.16	13.0	1.94	9.06	2.65	0.94	3.12	0.52	3.27	0.70	1.94
TM-06-245	7.8	0.074	160	5.84	12.4	1.87	8.83	2.56	0.94	3.00	0.50	3.20	0.68	1.90
TM-06-243	14.5	0.239	208	7.36	15.4	2.27	10.5	2.96	0.99	3.43	0.58	3.66	0.77	2.19
Hawaiian Rock Standard														
Kil1919[a]	9.5	0.095	133	15.9	38.4	5.54	25.0	6.40	2.14	6.54	1.01	5.65	1.05	2.59
±	0.1	0.002	0	0.0	0.0	0.06	0.1	0.04	0.06	0.01	0.01	0.05	0.01	0.01
Kil1919[b]	9.8	0.093	131	15.4	38.2	5.51	24.5	6.12	2.08	6.26	0.91	5.29	0.98	2.53

Sample	Tm	Yb	Lu	Th	Y	Nb	Hf	U	Pb	Ta	Zr	Sr	Sc
South Pagan post-caldera													
TM-06-275	0.38	2.46	0.39	1.24	24.7	1.94	2.16	0.611	3.23	0.13	96.2	294	23.1
TM-06-214	0.38	2.48	0.39	1.23	25.0	1.98	2.13	0.625	3.30	0.13	95.7	315	24.0
TM-06-24	0.36	2.34	0.37	1.09	23.8	1.82	1.95	0.550	2.93	0.12	87.8	337	21.7
TM-06-18	0.58	3.78	0.60	2.30	36.7	3.53	3.83	1.12	4.49	0.24	170	256	15.0
South Pagan pre-caldera													
TM-06-05	0.44	2.80	0.45	1.30	27.6	2.20	2.39	0.639	1.29	0.14	104	322	17.5
TM-06-202	0.36	2.29	0.37	1.01	23.0	1.80	1.82	0.474	2.51	0.12	78.5	318	22.7
CVR Dike													
TM-06-217	0.24	1.43	0.23	0.45	15.1	0.69	0.78	0.198	1.24	0.042	31.8	369	33.7
Late-Stage CVR													
TM-06-03	0.43	2.80	0.46	1.27	27.6	2.09	2.17	0.608	2.25	0.14	96.8	347	17.0
TM-06-34	0.36	2.33	0.37	0.92	23.4	1.68	1.71	0.432	2.70	0.11	74.9	367	22.8
Central Volcanic Region													
TM-06-216	0.32	2.01	0.32	0.69	20.8	1.03	1.08	0.282	2.14	0.060	44.5	408	27.2
TM-06-236	0.29	1.79	0.29	0.73	18.6	0.97	0.96	0.282	1.78	0.057	39.8	441	27.1
TM-06-237	0.30	1.88	0.30	0.69	19.3	0.99	1.03	0.300	2.59	0.058	42.1	435	28.5
TM-06-239	0.28	1.80	0.29	0.74	18.6	1.07	0.99	0.325	2.66	0.060	42.1	496	22.2
TM-06-245	0.28	1.76	0.28	0.69	18.1	1.00	0.95	0.312	2.26	0.055	39.7	487	22.1
TM-06-243	0.32	2.08	0.33	1.02	20.7	1.56	1.47	0.476	2.96	0.10	64.0	420	21.0
Hawaiian Rock Standard													
Kil1919[a]	0.34	1.95	0.29	1.30	26.9	19.4	3.77	0.460	1.11	1.47	180	406	24.3

Table 2 continued

Sample	Tm	Yb	Lu	Th	Y	Nb	Hf	U	Pb	Ta	Zr	Sr	Sc
±	0.00	0.01	0.00	0.00	0.4	0.2	0.02	0.003	0.00	0.00	2	0	0.4
Kil1919[b]	0.35	2.02	0.28	1.25	28.0	18.2	4.47	0.441	–	–	178	–	–

Values are in ppm

[a] Kil1919 ($n = 2$) was analyzed as an unknown with these analyses

[b] Reference values for Kil1919 are from Pietruszka and Garcia (1999). The ±value shows the range of the duplicate analyses of Kil1919

Table 3 Pb, Sr, and Nd isotopic data for southern Pagan lavas

Sample	$^{206}Pb/^{204}Pb$	$^{207}Pb/^{204}Pb$	$^{208}Pb/^{204}Pb$	$^{87}Sr/^{86}Sr$	$^{143}Nd/^{144}Nd$	ε_{Nd}
South Pagan post-caldera						
TM-06-275	18.8242	15.5633	38.4172	0.703495	0.512999	+7.05
TM-06-911	18.8225	15.5640	38.4179	0.703494	0.512996	+6.98
TM-06-214	18.8242	15.5626	38.4162	0.703479	0.513006	+7.17
TM-06-24	18.8233	15.5619	38.4141	0.703455	0.513007	+7.20
TM-06-18	18.8230	15.5651	38.4271	0.703467	0.512998	+7.02
South Pagan pre-caldera						
TM-06-05	18.8245	15.5657	38.4282	0.703447	0.513011	+7.28
TM-06-202	18.8294	15.5656	38.4330	0.703460	0.513004	+7.13
TM-06-205	18.8282	15.5640	38.4278	0.703457	0.513012	+7.30
CVR Dike						
TM-06-217	18.8505	15.5588	38.4166	0.703436	0.512976	+6.59
Late-Stage CVR						
TM-06-03	18.8086	15.5660	38.4225	0.703401	0.513001	+7.09
TM-06-34	18.8638	15.5611	38.4388	0.703407	0.513004	+7.14
Central Volcanic Region						
TM-06-216	18.8221	15.5650	38.4280	0.703441	0.513000	+7.06
TM-06-237	18.8310	15.5672	38.4361	0.703419	0.512982	+6.70
TM-06-245	18.8359	15.5668	38.4381	0.703466	0.512967	+6.41
TM-06-243	18.8487	15.5685	38.4561	0.703467	0.512980	+6.67
Hawaiian Rock Standard						
Kil1919	18.6550 ± 18	15.4895 ± 13	38.2059 ± 37	–	0.512974 ± 4	+6.52

Lead isotopic ratios were corrected for instrumental mass fractionation using the measured isotopic ratio of Tl (NBS 997) added to the sample compared to an assumed $^{205}Tl/^{203}Tl = 2.3889$ for this standard from Thirlwall (2002). The average Tl-corrected value for NBS981 Pb ($n = 20$) was $^{206}Pb/^{204}Pb = 16.9419 \pm 16$ (2σ), $^{207}Pb/^{204}Pb = 15.4991 \pm 18$ (2σ), and $^{208}Pb/^{204}Pb = 36.7216 \pm 53$ (2σ). All of the Pb isotopic data are reported relative to the NBS 981 Pb standard values of Galer and Abouchami (1998): $^{206}Pb/^{204}Pb = 16.9405$, $^{207}Pb/^{204}Pb = 15.4963$, and $^{208}Pb/^{204}Pb = 36.7219$. Sr and Nd isotopic ratios were corrected for instrumental mass fractionation relative to $^{86}Sr/^{88}Sr = 0.1194$ and $^{146}Nd/^{144}Nd = 0.7219$, respectively. The average measured values for Sr and Nd standards were $^{87}Sr/^{86}Sr = 0.710244 \pm 10$ (2σ; $n = 10$) for SRM987 (by TIMS) and $^{143}Nd/^{144}Nd = 0.512097 \pm 8$ (2σ; $n = 8$) for Ames Nd (by MC-ICP-MS). All Sr and Nd isotopic data are reported relative to constant standard values for SRM987 ($^{87}Sr/^{86}Sr = 0.710250$) and Ames Nd ($^{143}Nd/^{144}Nd = 0.512130$). After correcting to this value for Ames Nd, multiple analyses of the La Jolla Nd standard ($n = 4$) run as an unknown averaged $^{143}Nd/^{144}Nd = 0.511843 \pm 7$. Averages of multiple analyses of the Kil1919 rock standard for Pb ($n = 8$) and Nd ($n = 7$) isotopic ratios are given. The uncertainties on the Kil1919 Pb and Nd isotopic ratios are the $\pm 2\sigma_m$ errors of the replicate analyses. Strontium isotopic ratios are an average of duplicate analyses of each sample (except TM-06-911; $n = 3$). Total procedural blanks were negligible compared to the amount of sample used (>0.6 g) and the concentrations of Pb, Sr, and Nd in the samples

(MC-ICP-MS), whereas Sr isotopic ratios were measured using a VG Sector 54 thermal ionization mass spectrometer (TIMS; Table 3). All literature isotopic data shown on the figures and discussed in the text has been corrected relative to the isotopic standards listed in Table 3.

Results

Major elements

South Pagan and CVR lavas are subalkaline, medium-K basalts to high-silica andesites (48–62 wt. % SiO_2) with low

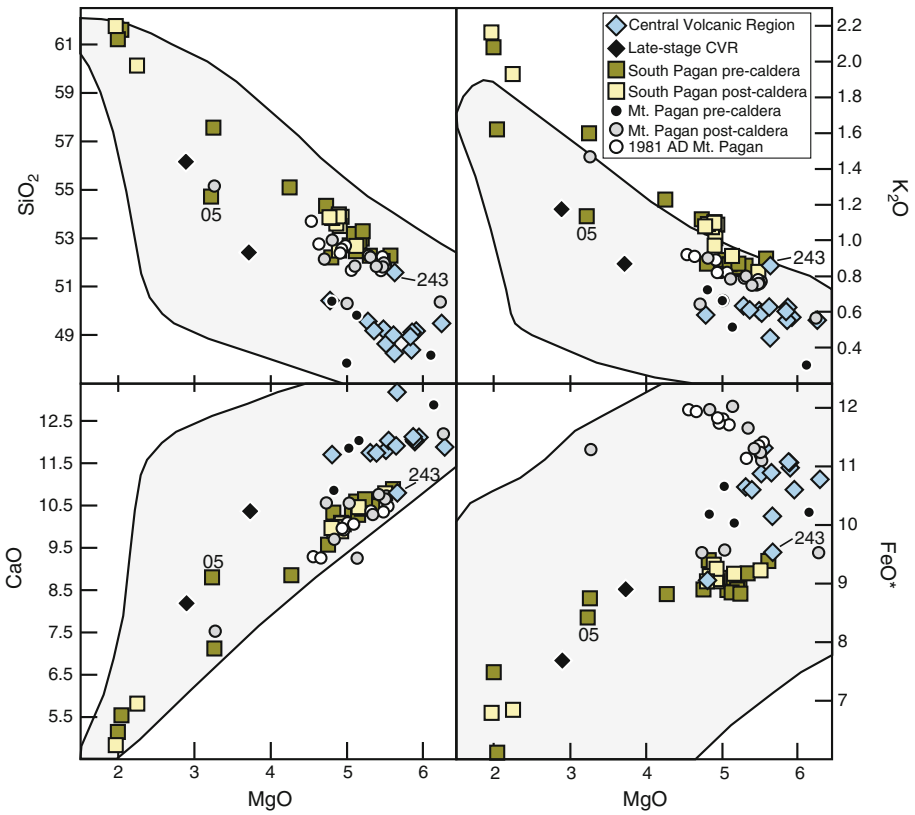

Fig. 3 Whole-rock MgO variation diagrams for South Pagan, CVR, and Mt. Pagan lavas. The compositional field of other Mariana arc lavas is shown in the *light gray area*. The lavas are grouped according to eruptive stages (see *key* for *symbols*). All values are in wt. %. The data sources for Mt. Pagan and Mariana lavas are from Larson et al. (1974), Dixon and Batiza (1979), Meijer and Reagan (1981), Woodhead (1989) and Elliott et al. (1997). The *error bars* are equal to or less than the size of the *symbols*

to moderate MgO contents (2.0–6.3 wt. % MgO; Fig. 3). These lavas have major element compositions that mostly lie within the range of lavas from other Mariana volcanoes (e.g., Woodhead 1989). The CVR lavas ($n = 15$) are basalts with a relatively narrow MgO range (4.8–6.3 wt. %), except for the two evolved late-stage samples (2.9 and 3.7 wt. %). South Pagan lavas ($n = 27$) are basaltic andesites to high-silica andesites with 2.0–5.6 wt. % MgO. South Pagan and CVR lavas generally plot on distinct major element trends (Fig. 3). The CVR lavas have higher CaO, FeO, and Al_2O_3 (not shown), and lower SiO_2 and K_2O contents (at a given MgO) except for the oldest stratigraphically controlled CVR lava (TM-06-243) and a South Pagan pre-caldera flow (TM-06-05) that seem to lie along the South Pagan and CVR trends, respectively (Fig. 3). South Pagan and CVR lavas display overlapping TiO_2, P_2O_5, and Na_2O contents at a given MgO (Table 1). The major element abundances of Mt. Pagan lavas are similar to South Pagan and CVR lavas. In detail, Mt. Pagan pre-caldera lavas typically overlap with CVR lavas, whereas most Mt. Pagan post-caldera lavas lie along trends (except for FeO which is highly variable) that are similar to South Pagan lavas (Fig. 3).

Trace elements

Normalized trace element patterns for South Pagan and CVR lavas relative to average normal mid-oceanic ridge basalt (N-MORB; Hofmann 1988) are similar to other Mariana arc lavas (Fig. 4). South Pagan and CVR lavas are enriched in Th, U, Pb, and large ion lithophile elements (LILE: Rb, Ba, K, Sr), and depleted in high field strength elements (HFSE: Nb, Ta, Hf, Zr) with respect to N-MORB. South Pagan and CVR lavas are slightly enriched in most

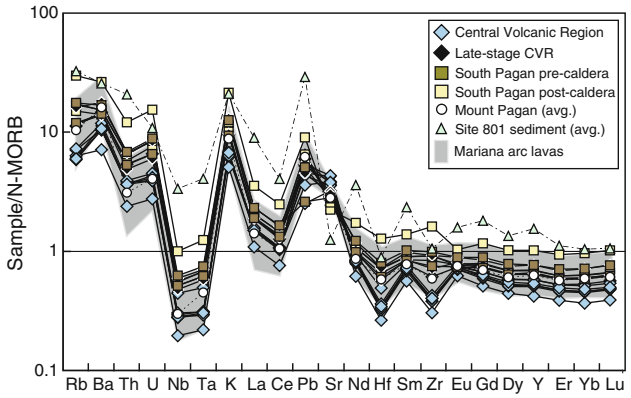

Fig. 4 Trace element patterns for Pagan lavas normalized to N-MORB (Hofmann 1988). The Mt. Pagan pattern (*open circles*) is an average of six pre- and post-caldera lavas from Woodhead (1989) and Elliott et al. (1997). The pattern for average ODP Site 801 sediment (*triangles*) is from Plank and Langmuir (1998). The range of normalized trace element abundances of other Mariana lavas is shown in the *gray field* (Woodhead 1989; Elliott et al. 1997). The other *symbols* are defined in the *key*

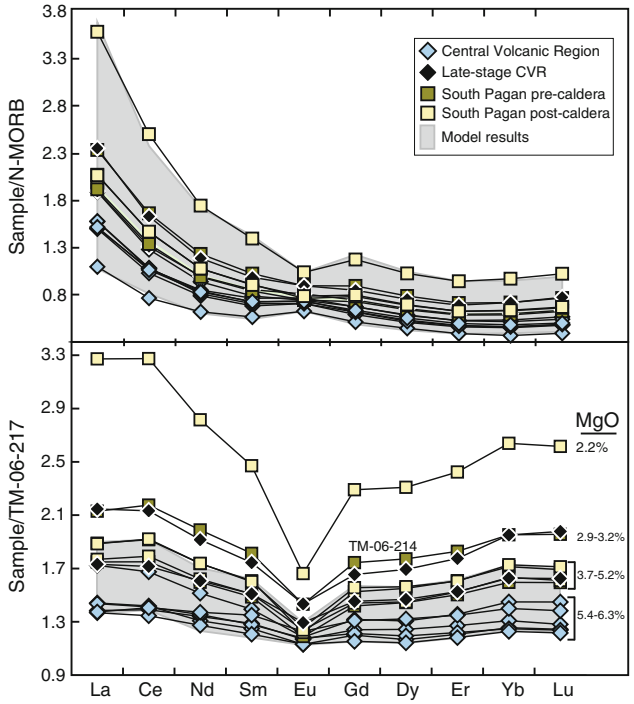

Fig. 5 Rare earth element abundances in CVR and South Pagan lavas normalized to N-MORB (Hofmann 1988) and a CVR sample (TM-06-217). Sample TM-06-217 was chosen because it is relatively mafic (5.7 wt. % MgO) and is thought to result from a low degree of partial melting (3.2%) of a sediment-poor (0.9%) source (Table A2—Electronic Supplementary Material) compared to other Pagan lavas. Thus, other Pagan lavas will tend to have a more saucer-shaped REE pattern relative to sample TM-06-217. The *gray field* shows the range of the REE mass-balance mantle source and melting model results for CVR and South Pagan lavas with >3.5% MgO (Table 5). The *symbols* are defined in the *key*

of the light rare earth elements (LREE: La, Ce, Pr, Nd) compared to N-MORB, but have relatively constant or slightly decreasing abundances of the middle (MREE: Sm, Eu, Gd, Tb, Dy, Ho, Er) to heavy (HREE: Tm, Yb, Lu) rare earth elements, which are slightly more depleted than N-MORB (Fig. 4). The REE abundances of CVR and South Pagan lavas normalized to N-MORB or some other Pagan lavas (e.g., CVR sample TM-06-217) produce saucer-shaped REE patterns (Fig. 5). Most South Pagan lavas display negative Eu anomalies, which are larger for the lower MgO samples (Fig. 5).

South Pagan and CVR lavas display small but systematic differences in key trace element ratios (Fig. 6). The CVR lavas (excluding late-stage lavas) have higher Ba/Th, Sm/Yb, La/Nb, Th/Nb, and Nb/Zr ratios on average than South Pagan lavas. In contrast, ratios of LREE to MREE or HREE (e.g., La/Sm) in CVR lavas typically overlap with South Pagan lavas and extend to lower values (on average). In addition, some of these ratios (e.g., Ba/Th and Nb/Zr) have generally decreased over the eruptive history of both volcanoes (Fig. 7). Mount Pagan lavas show differences in many of these key trace element ratios compared to South Pagan and CVR lavas, despite their close proximity (all within ~10 km). For example, South Pagan and CVR lavas have higher La/Sm, Sm/Yb, and Nb/Zr ratios, and significantly lower Ba/Th and Ba/La than those of Mt. Pagan lavas (Fig. 6).

Pb, Sr, and Nd isotopes

South Pagan and CVR lavas lie mostly within the Pb, Nd, and Sr (not shown) isotopic range of other Mariana lavas (Fig. 8). The Pb isotopic ratios of CVR ($^{206}Pb/^{204}Pb$ = 18.81–18.86) and South Pagan ($^{206}Pb/^{204}Pb$ = 18.82–18.83) lavas display an extremely limited range, compared to Mt. Pagan lavas ($^{206}Pb/^{204}Pb$ = 18.62–18.86). The ranges of $^{143}Nd/^{144}Nd$ in South Pagan (0.51300–0.51301) and CVR (0.51297–0.51300) lavas (Fig. 9) are also smaller than Mt. Pagan lavas (0.51300–0.51306). The $^{206}Pb/^{204}Pb$ and $^{208}Pb/^{204}Pb$ ratios of South Pagan and CVR lavas have generally decreased over the eruptive history of both volcanoes (Figs. 7, 9a). South Pagan and CVR lavas are isotopically distinct (in $^{206}Pb/^{204}Pb$ vs. $^{143}Nd/^{144}Nd$ space) from Mt. Pagan lavas, except for three Mt. Pagan post-caldera lavas that lie within analytical uncertainty (Fig. 9b). Mount Pagan pre-caldera and 1981 A.D. lavas display relatively high $^{143}Nd/^{144}Nd$ and low $^{206}Pb/^{204}Pb$ ratios, whereas CVR lavas have relatively low $^{143}Nd/^{144}Nd$ and high $^{206}Pb/^{204}Pb$ ratios (Fig. 9b). South Pagan and late-stage CVR lavas and some Mt. Pagan post-caldera flows have relatively high $^{206}Pb/^{204}Pb$ and intermediate $^{143}Nd/^{144}Nd$ ratios that lie between the fields of CVR and other Mt. Pagan lavas. The $^{87}Sr/^{86}Sr$ ratios for South Pagan and CVR lavas (0.70340–0.70350) partially overlap with the range of Mt. Pagan lavas (0.70345–0.70354, Woodhead 1989; Elliott et al. 1997), although no systematic temporal variations are evident in the data (Table 3).

Discussion

Magmatic differentiation

The relatively wide range of MgO (2.0–6.3 wt. %) and SiO_2 (48–62 wt. %) contents, and the presence of olivine, clinopyroxene, plagioclase, and titanomagnetite phenocrysts in South Pagan and CVR lavas suggest that their parental magmas were modified by variable amounts of crystal fractionation. Moreover, the high abundance of complexly zoned and sieved plagioclase phenocrysts (~15–40 vol.%), and minor plagioclase xenocrysts in most of these lavas indicates that magma mixing was also important. South Pagan and CVR lavas show a

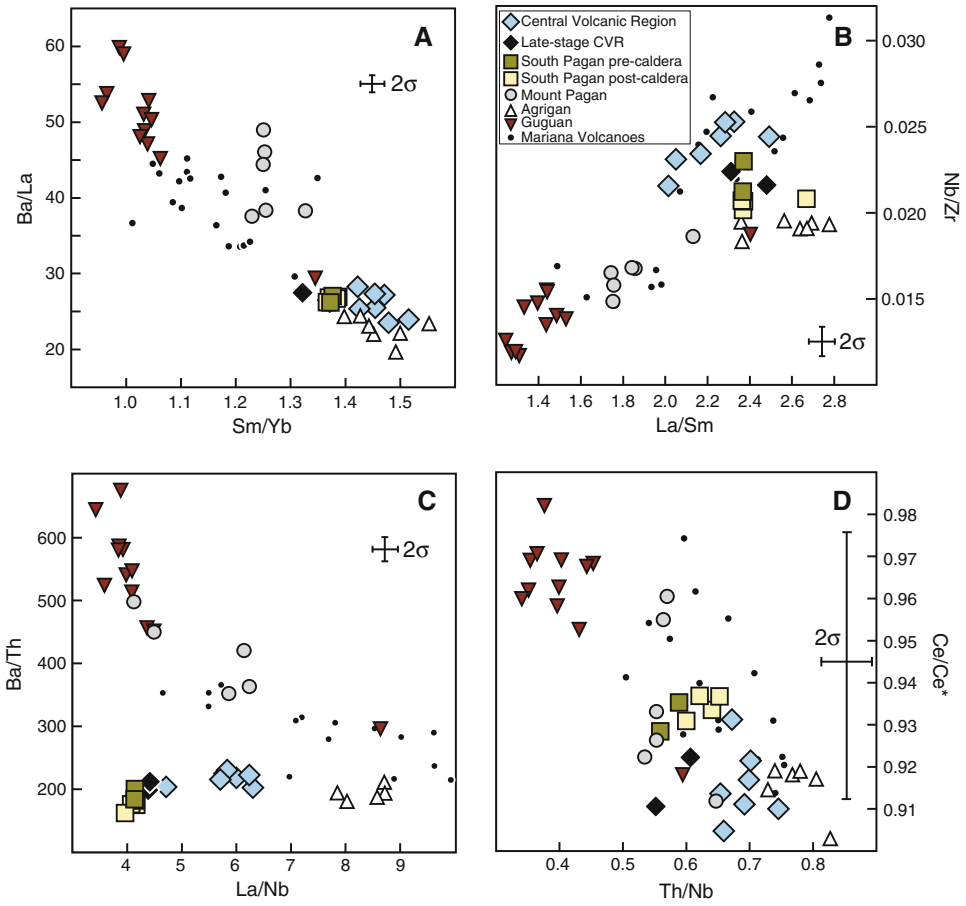

Fig. 6 Trace element ratio–ratio plots for Pagan lavas. The compositions of Mt. Pagan (*gray circles*), Guguan (*upside down triangles*), Agrigan (*white triangles*), and Mariana volcanoes (*small black circles*) are shown, using data from Woodhead (1989), Elliott et al. (1997), and Stern et al. (2006). The Ce/Ce* ratio is the measured Ce concentration divided by the expected Ce concentration (Ce*), both normalized to primitive mantle (Sun and McDonough 1989). Ce* is calculated from the interpolation of primitive mantle-normalized abundances of the rare earth elements La and Pr. The 2σ *error bars* for South Pagan and CVR lavas are shown in each plot. The Ce/Ce* *error bar* is probably an overestimate of the actual uncertainty. The other *symbols* are defined in the *key*

strong decrease in CaO/Al_2O_3, Sr/La and Eu/Eu*, and FeO and TiO_2/Y with increasing SiO_2 (Figs. 3, 10), which is consistent with the overall fractionation of clinopyroxene, plagioclase, and titanomagnetite, respectively. The abundances of incompatible elements (e.g., HFSE, LREE, and LILE) in South Pagan and CVR lavas increase with the extent of differentiation (e.g., K_2O vs. MgO; Fig. 3), although ratios of most incompatible elements show little or no correlation with indices of differentiation.

The amount of clinopyroxene fractionation in South Pagan (7–26%) and CVR (0.5–5%) lavas was estimated based on mass-balance calculations assuming a parental magma with a CaO/Al_2O_3 ratio equal to the highest value observed for Pagan lavas (0.7; Woodhead 1989). The composition of clinopyroxene used in the calculation ($CaO = 22$ wt. %, $Al_2O_3 = 1.9$ wt. %) is an average of multiple mineral core analyses from Guguan lavas (Kohut et al. 2006). Although plagioclase fractionation or accumulation can also modify the CaO/Al_2O_3 ratios of the lavas, mass-balance calculations indicate that the effect of plagioclase fractionation on the CaO/Al_2O_3 ratio is only $\sim$25% that of an equivalent amount of clinopyroxene fractionation. Furthermore, the CaO/Al_2O_3 ratios in South Pagan and CVR lavas also correlate strongly with their Sc/Y ratios (not shown), which is a tracer of clinopyroxene fractionation (e.g., Naumann and Geist 1999). The good linear correlation between these two ratios ($R^2 = 0.92$) suggests that the CaO/Al_2O_3 ratio is dominantly controlled by clinopyroxene fractionation.

The extent of plagioclase and titanomagnetite crystallization in Pagan lavas was estimated using an equilibrium crystallization model (Shaw 1970) assuming that the highest Sr/La (89; Woodhead 1989) and TiO_2/Y (450; this study) ratios observed in Pagan lavas represent a parental melt composition. The mineral/melt partition coefficients used for Sr, La, Ti, and Y are listed in Table 4. The results show that the greatest amounts of plagioclase fractionation occurred in the South Pagan lavas (36–47%, excluding sample TM-06-18 with 70%) and late-stage CVR lavas (31 and 44%), compared to the other CVR lavas (2–24%). Although plagioclase accumulation could also be an important process based on the relatively high modal abundance of this mineral in Pagan lavas, most lavas have Eu/Eu* < 1, which indicate that plagioclase fractionation dominates. The calculated amount of titanomagnetite

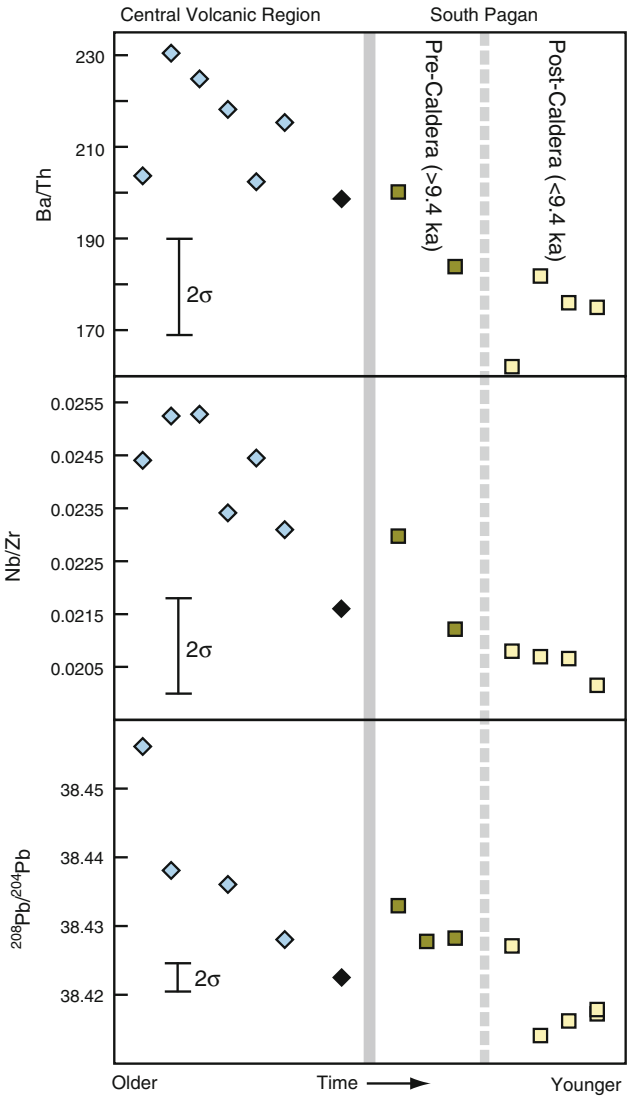

Fig. 7 Temporal geochemical variations of South Pagan and CVR lavas. The *dashed gray vertical lines* denote the boundaries between the South Pagan pre- and post-caldera stages. The *solid line* marks the boundary between CVR and South Pagan pre-caldera lavas. The *symbols* are defined in the caption to Fig. 3. The 2σ *error bars* are shown on each plot

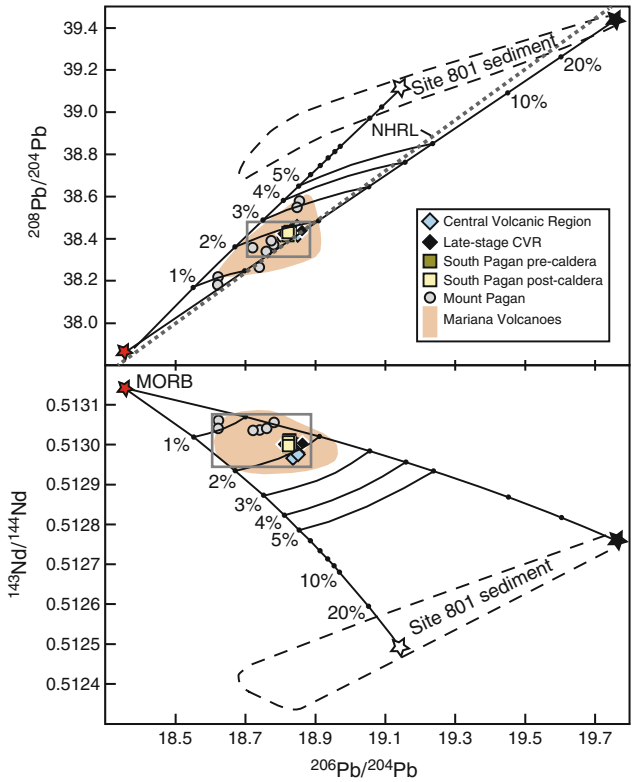

Fig. 8 ^{206}Pb/^{204}Pb versus ^{208}Pb/^{204}Pb and ^{143}Nd/^{144}Nd ratios for South Pagan and CVR lavas compared with Mt. Pagan (*gray circles*) and Mariana (*tan fields*) lavas, and subducted sediment from ODP Site 801 (Plank and Langmuir 1998). The *rectangles* outline the enlarged views presented in Fig. 9. The N-MORB composition (*red star*) is an average from Bach et al. (1994), Mahoney et al. (1994), Vlastevic et al. (1999), Wendt et al. (1999), and Chauvel and Blichert-Toft (2001). The data sources for Mt. Pagan and the other Mariana lavas are given in the caption to Fig. 6. Mixing lines between regional subducted sediment (*black* and *white stars*) and average N-MORB are shown. The sediment end members include average bulk sediment (excluding the pelagic clay unit) from ODP Site 801 and a volcanic turbidite sample from ODP Site 801 with the most radiogenic Pb isotopic ratios (*black star*). The Pb and Nd concentrations used in the mixing model lie within the range observed for ODP Site 801 sediment (10 and 90 ppm, respectively) and N-MORB (0.3 and 4 ppm, respectively). The amount of sediment mixing with N-MORB is shown in 1% increments. The sediment contributions were estimated from the intersection of contours in 0.1% increments (not shown). The Northern Hemisphere Reference (NHRL) line from Hart (1984) is shown for comparison. The other *symbols* are defined in the *key*. The 2σ *error bars* are smaller than the size of the symbols

crystallization in the South Pagan lavas (3–16%) is higher than CVR lavas (0–3%).

The effects of crystal fractionation and magma mixing in Pagan lavas are superimposed on the long-term differences in the composition of the parental magmas delivered to each of the three volcanoes. This interpretation is supported by the small, but significant differences in ratios of key incompatible trace elements (Fig. 6), and Pb and Nd isotopic ratios (Fig. 9) between CVR, South Pagan, and Mt. Pagan lavas. In the following sections, we discuss the origin of these parental magma differences.

The role of slab contributions

Aqueous fluid component

Dehydration reactions in the downgoing slab are expected to transfer elements that are mobile in an aqueous fluid phase into the overlying mantle wedge (Arculus and Johnson 1981). Large ion lithophile elements are fluid mobile and are readily partitioned into this aqueous fluid (Gill 1981; Hawkesworth et al. 1991; Keppler 1996;

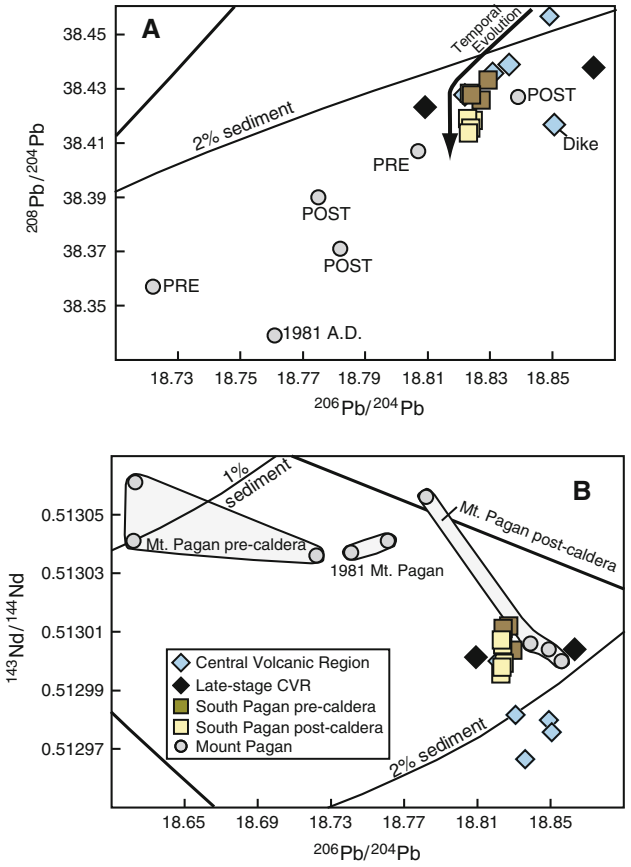

Fig. 9 $^{206}Pb/^{204}Pb$ versus $^{208}Pb/^{204}Pb$ and $^{143}Nd/^{144}Nd$ ratios for South Pagan, CVR, and Mt. Pagan lavas. The *two panels* presented here correspond to the rectangular outlines in Fig. 8. Mount Pagan samples labeled PRE and POST refer to pre- and post-caldera stage lavas, respectively. The *arrow* illustrates the systematic variation of CVR and South Pagan lavas toward lower Pb isotopic ratios with time. The data sources and mixing line calculations are presented in the caption to Fig. 8. The other *symbols* are defined in the *key*. The 2σ *error bars* on each panel are the size of the *symbols* or smaller

Johnson and Plank 1999), whereas REE, HFSE, and Th are relatively immobile in aqueous fluids (Brenan et al. 1995; Keppler 1996; Ayers et al. 1997; Kessel et al. 2005). Partial melting of the mantle wedge (enriched in these fluid mobile elements) produces magmas with elevated ratios of highly incompatible LILE over HFSE, LREE, or Th (e.g., Ba/La, or Ba/Th). Thus, variations in the Ba/Th and Ba/La ratios of Pagan and other Mariana lavas are thought to be dominantly controlled by the relative amount of the fluid component in the mantle source region (e.g., Elliott et al. 1997; Stern et al. 2006).

South Pagan and CVR lavas have low Ba/Th and Ba/La ratios compared to most other Mariana lavas (Fig. 6), indicating these lavas originated from a source that experienced relatively small amounts of fluid addition. These lavas display small temporal decreases in Ba/Th ratios, suggesting that the amount of the fluid component has diminished during the eruptive history of these two volcanoes (Fig. 7). Mt. Pagan lavas display Ba/Th and Ba/La ratios that are 2–3 times higher than the values for CVR and South Pagan lavas. Moreover, these trace element ratios in Mt. Pagan lavas overlap with lavas from Guguan (Fig. 6), the fluid-rich end member for Mariana lavas (Kent and Elliott 2002). Thus, Mt. Pagan magmas probably originated from a source with a larger fluid component than CVR and South Pagan lavas.

Sediment component

The amount of subducted sediment transferred to the depleted mantle wedge is generally estimated as <2–3% for intra-oceanic arcs, including the Mariana arc (e.g., Meijer 1976; Turner and Hawkesworth 1997; George et al. 2003; Wade et al. 2005; Stern et al. 2006). These estimates are primarily based on ratios of fluid-immobile incompatible elements (i.e., HFSE, REE, and Th), and Pb, Hf, and Nd isotopic ratios. Bulk seafloor sediment collected ~900 km east of Pagan at ODP Site 801 is thought to represent the composition of sediment that is subducted beneath the Marianas (Plank and Langmuir 1998). On average, this sediment has low Nd and high Pb isotopic ratios (Fig. 8), high abundances of highly incompatible elements (Fig. 4), and a prominent negative Ce anomaly (Plank and Langmuir 1998) compared to N-MORB. Consequently, these geochemical signatures and elevated ratios of highly to moderately incompatible elements (i.e., Th/Nd, La/Sm, Th/Nb, and Nb/Zr) in Mariana arc lavas are thought to result from the contribution of sediment to the mantle wedge (Elliott et al. 1997; Elburg and Foden 1998; Kohut et al. 2006).

Subducted sediment may be transferred to the mantle wedge as bulk sediment from the downgoing slab or as a partial melt (e.g., George et al. 2003). For example, Th/Nd versus $^{143}Nd/^{144}Nd$ variations in arc lavas (Fig. 11) has been used to assess whether sediment is added to the mantle wedge in bulk or as a partial melt (e.g., Class et al. 2000; Hochstaedter et al. 2001; Jicha et al. 2004; Dufrane et al. 2009). The CVR and Mt. Pagan lavas plot close to mixing arrays between a depleted end member (N-MORB) and Site 801 bulk sediment, whereas South Pagan and late-stage CVR lavas have Th/Nd ratios that are too high to be explained solely by bulk sediment addition (Fig. 11). Instead, the relatively high Th/Nd ratios of the South Pagan and late-stage CVR lavas could reflect mixing between a depleted end member (N-MORB) and a 20% partial melt of Site 801 sediment (Fig. 11). Rutile is thought to be an important accessory mineral in Mariana subducted sediment (Elliott et al. 1997; Tollstrup and Gill 2005). Partial melting of rutile-bearing sediment in the mantle source would also fractionate HFSE from REE and Th if it

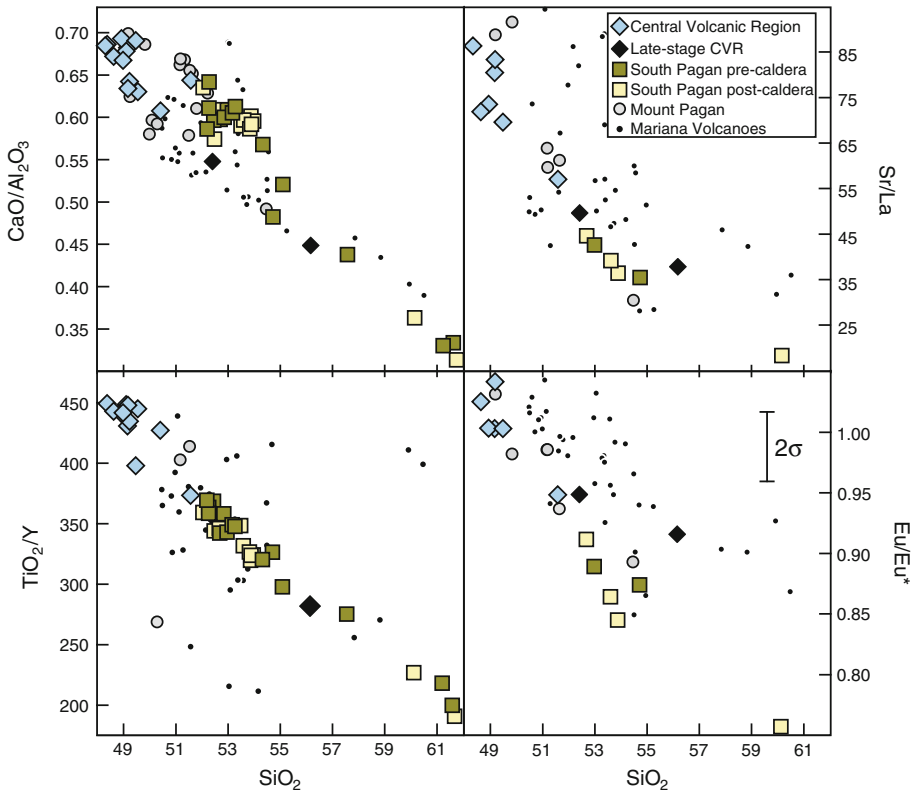

Fig. 10 SiO_2 versus CaO/Al_2O_3, Sr/La, TiO_2/Y, and Eu/Eu* (Eu anomaly) for Pagan lavas. The Eu/Eu* ratio is the measured Eu concentration over the expected Eu concentration (Eu*). Eu* is calculated from the interpolation of primitive mantle-normalized abundances of the rare earth elements Sm and Gd. Data sources for the Mariana lavas are given in the caption to Fig. 6. The *symbols* are defined in the *key*. The 2σ *error bars* are the size of the *symbols* or smaller except for the Eu/Eu* ratio

remained in the residue of partial melting. This process would lead to higher Th/Nb and La/Nb ratios than expected for addition of bulk sediment alone (Kent and Elliott 2002; George et al. 2003).

The CVR lavas have the lowest $^{143}Nd/^{144}Nd$ and Ce/Ce* ratios, and highest Th/Nb and Nb/Zr ratios among Pagan lavas (Figs. 6, 9), which probably reflects a greater amount of sediment in their source. These ratios in the CVR lavas are similar to Agrigan lavas, which are thought to represent the sediment-rich end member for Mariana volcanoes (Kent and Elliott 2002). Although some sediment indicators overlap between South Pagan and CVR lavas (i.e., La/Sm), South Pagan lavas (on average) have higher $^{143}Nd/^{144}Nd$ ratios, lower Pb isotopic ratios and Th/Nb, Nb/Zr, and La/Nb ratios, and Ce/Ce* values closer to unity, indicating a smaller sediment contribution to their source compared to CVR lavas. Mount Pagan lavas display higher $^{143}Nd/^{144}Nd$ ratios, and lower Nb/Zr, La/Sm and Pb isotopic ratios compared to South Pagan and CVR lavas. Many of these ratios in Mt. Pagan lavas also partially overlap with the compositional field of Guguan lavas, which are thought to represent the sediment-poor end member for Mariana volcanoes (Stern et al. 2006). Overall, these observations suggest that most Mt. Pagan lavas were derived from a more sediment-poor source than CVR and South Pagan lavas (Figs. 6, 9).

Table 4 Mineral/melt partition coefficients used for the mass-balance model calculations

	Magnetite	Clinopyroxene	Orthopyroxene	Plagioclase
La	0	0.12	0.02	0.036
Ce	0	0.12	0.03	0.031
Nd	0	0.22	0.04	0.025
Sm	0	0.31	0.05	0.020
Eu	0	0.31	0.06	0.330
Gd	0	0.39	0.07	0.016
Dy	0	0.53	0.11	0.013
Er	0	0.63	0.13	0.010
Yb	0	0.70	0.15	0.007
Lu	0	0.70	0.16	0.005
Ti	8	–	–	–
Y	0.004	–	–	–
Sr	–	–	–	1.8

Magnetite, olivine, and spinel. The mineral/melt partition coefficients (D) for the REE are expected to be very low in these minerals (Nielsen et al. 1992) and are assumed to be zero. For magnetite, D_{Ti} comes from Nielsen (1992), and D_Y is from Nielsen et al. (1992). Clinopyroxene. D_{Ce}, D_{Nd}, D_{Sm}, D_{Er}, D_{Yb}, D_{Lu} used in the model were selected to lie within the range of the experimental results from Salters and Longhi (1999). Orthopyroxene. D_{La}, D_{Sm}, and D_{Gd} are average values from Nielsen et al. (1992). Plagioclase. D_{La}, D_{Ce}, D_{Sm}, D_{Gd}, and D_{Yb} are from the experimental results of Phinney and Morrison (1990). D_{Sr} and D_{Eu} are from Pietruszka and Garcia (1999). All other partition coefficients are interpolated or extrapolated from these values

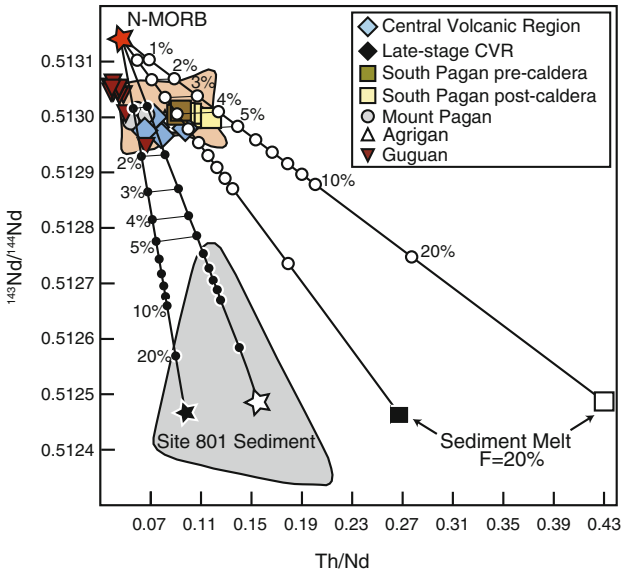

Fig. 11 Th/Nd versus $^{143}Nd/^{144}Nd$ for Mariana lavas. Mixing lines between average N-MORB (*red star*) and bulk sediment from ODP site 801 (*black* and *white stars*) and sediment melts (*black* and *white squares*) are shown. Two types of bulk sediment are shown: an average of all sediment units from site 801 (*white star*) and an average excluding the upper pelagic clay unit (*black star*). The $^{143}Nd/^{144}Nd$ ratio and Nd concentrations used for the N-MORB end member and bulk sediment end members are listed in the caption to Fig. 8. The Th concentrations used for the N-MORB end member is 0.19 ppm (Hofmann 1988), whereas the average bulk site 801 sediment (8.8 ppm) and the bulk site 801 sediment excluding the pelagic clay unit (14.1 ppm) end members were calculated from the Nd concentrations used for the mixing lines in Fig. 8 and the average Th/Nd ratio of each type of sediment (Plank and Langmuir 1998). Each of these sediment compositions were partially melted 20% (*black* and *white squares*) using the 800°C bulk partition coefficients from Johnson and Plank (1999). The batch melting equation was used for this calculation (Shaw 1970). The mixing lines between N-MORB and the bulk sediment and sediment melt end members are labeled in 1% increments. Data sources for the Mariana lavas are given in the caption to Fig. 6. The *symbols* are defined in the *key*. The 2σ *error bars* are smaller than the size of the *symbols*

Lead and Nd isotopic arrays of arc lavas that trend from MORB-like compositions toward average local sediment have been recognized at several arcs, including the Marianas (Jicha et al. 2004; Tollstrup and Gill 2005; Marchesi et al. 2007). These trends are thought to result from partial melting of a variably mixed source of depleted mantle and enriched sediment. To quantify the extent of sediment addition to the source of Pagan, Agrigan, and Guguan lavas, mixing lines were calculated between two ODP Site 801 sediment end members and average N-MORB (Figs. 8, 9). The first sediment end member is average Site 801 bulk sediment (excluding a pelagic clay unit). The pelagic clay unit represents the upper 65 m of the stratigraphic section, which may have been scraped off from the down going plate as it entered the trench (Wade et al. 2005). The second sediment end member is a volcanic turbidite sample from Site 801 with highly radiogenic Pb isotopic ratios. The amount of sediment was estimated from the $^{206}Pb/^{204}Pb$ versus $^{143}Nd/^{144}Nd$ plot (Fig. 9b) because it is thought to be more accurate than the $^{206}Pb/^{204}Pb$ plot versus $^{208}Pb/^{204}Pb$ plot. The sediment contribution to CVR lavas (~1.9–2.2%, with an average of 2.1%, excluding late-stage flows) is slightly higher on average than South Pagan lavas (~1.8–1.9%, with an average of 1.8%). This observation is consistent with the temporal decreases in some sediment indicators (e.g., Nb/Zr and $^{208}Pb/^{204}Pb$) during the eruptive history of both volcanoes (Fig. 7). Mount Pagan lavas generally require a smaller amount of sediment (~0.8–1.9%, with an average of 1.4%). The sediment contribution for Agrigan and Guguan lavas was also calculated using the Pb and Nd isotopic ratios from Woodhead (1989), Elliott et al. (1997), and Stern et al. (2006). The sediment estimates for Pagan lavas generally lie between the average values of sediment-poor Guguan (~0.9–1.7%, with an average of 1.3%) and sediment-rich Agrigan (~1.5–2.1%, with an average of 2.0%) end member lavas.

Mantle source and melting model for Mariana lavas

Role of amphibole fractionation

Recent studies have noted the importance of amphibole fractionation in the crust and/or magmatic interaction with amphibole-bearing crustal gabbro cumulates as a control on the REE abundances of arc lavas (e.g., Macpherson et al. 2006; Davidson et al. 2007). For example, MREE (e.g., $D_{Dy} = 1.5$; Sisson 1994) are more compatible in hornblende than HREE ($D_{Yb} = 1.0$) and LREE ($D_{La} = 0.2$), suggesting that the saucer-shaped REE patterns observed in some arc lavas (e.g., Jolly et al. 2002; Figueroa et al. 2009) are related to parental magmas interacting with or fractionating amphibole. Similarly, some arc lavas display decreasing MREE/HREE (e.g., Dy/Yb) ratios with increasing differentiation, which is thought to result from amphibole fractionation or interaction (Macpherson et al. 2006; Davidson et al. 2007; Larocque and Canil 2010). The REE abundances of Pagan lavas normalized to N-MORB or a mafic (5.7 wt. % MgO) CVR sample (TM-06-217) display a saucer-shaped pattern (Fig. 5). However, no modal amphibole is observed in Pagan lavas, and this mineral is absent or only minimally present in other Mariana lavas and xenoliths (Dixon and Batiza 1979; Meijer and Reagan 1981; Kent and Elliott 2002). Moreover, Dy/Yb ratios of CVR and South Pagan lavas show little or no correlation with indices of differentiation (not shown). Given the lack of petrographic and geochemical evidence for amphibole in Pagan lavas, we

present a mass-balance mantle source and melting model to explain the saucer-shaped REE patterns of Pagan lavas.

Model description and results

The mass-balance model presented here considers the enriched sediment contribution to the depleted mantle wedge, variations in the degree of partial melting, and crystal fractionation of an amphibole-free mineral assemblage to explain the saucer-shaped REE patterns of Pagan lavas (Fig. 5). The geochemical effects of fluid addition to the mantle wedge were not modeled. This is possible for two reasons. First, the indices of fluid (e.g., Ba/Th) and sediment (e.g., La/Nb) addition to the source of Mariana lavas are decoupled (Fig. 6c). This is evidence for two discrete slab components that may be treated separately. Second, the REE are thought be relatively immobile in the presence of fluid (Brenan et al. 1995; Keppler 1996). The enriched sediment component will probably impart a much stronger geochemical signature on the REE abundances of the Mariana lavas. Therefore, we consider only bulk addition of sediment to the depleted mantle wedge. Representative lavas from the fluid-rich (Guguan) and sediment-rich (Agrigan) end members for Mariana arc lavas were also modeled. The model assumptions and parameters are described in Table 5. Briefly, this two-step model (Fig. 12) attempts to match the REE abundances of these lavas by: (1) partial melting a variably mixed source consisting of a small amount of subducted sediment (from ODP Site 801) and depleted mantle (DMM), and (2) fractionating or accumulating clinopyroxene, plagioclase, olivine, and titanomagnetite from these parental melts. The model results match the REE abundances of the least evolved Pagan, Agrigan, and Guguan lavas (with >3.5 wt. % MgO) within 8%, with an average difference of 2% for the modeled REE.

The model results (Table 5) demonstrate that the saucer-shaped REE patterns in Pagan lavas can arise from partial melting of mixed mantle-sediment source and that amphibole is not required to depress the MREE relative to the LREE and HREE. Two different factors create the saucer-shaped pattern. First, the addition of sediment to the DMM source creates a mixed source that is slightly less depleted in LREE (Fig. 12a) compared to DMM. Second, partial melting of this mixed source generates a melt that is slightly enriched in LREE, but with MREE abundances that better preserve the original DMM source pattern and remain more depleted than the HREE (Fig. 12b). Subsequent crystallization or accumulation of olivine, clinopyroxene, plagioclase, and titanomagnetite raises or lowers the REE patterns, although clinopyroxene removal can cause further LREE to HREE fractionation, and plagioclase fractionation can create negative Eu anomalies (Fig. 12b). However, the effect of clinopyroxene fractionation on the REE patterns is relatively minor. For example, the La/Yb ratio of the modeled sample with the greatest amount of clinopyroxene fractionation (16%) increases by only 10% from the parental melt. The calculated amount of crystal fractionation or accumulation in Mariana lavas broadly correlates with their SiO_2 (Fig. 13) and MgO (not shown) contents, which suggests that the model successfully accounts for the effects of magmatic differentiation.

The model results show that the average amount of sediment involved in the genesis of Guguan (~0.6%) and Mt. Pagan lavas (~0.9%) is lower than CVR (~1.4%), South Pagan (~1.8%), and Agrigan (~2.0%) lavas (Table 6). As expected, the indices of sediment addition (e.g., La/Sm or Th/Nb) show a positive correlation with the calculated amount of sediment (Fig. 14). Although the La/Sm ratio is model-dependant, the strong correlation between the calculated amount of sediment and the La/Sm ratios of the lavas illustrates that this ratio is a key sediment indicator in Mariana lavas. Moreover, the broad correlation between the calculated amount of sediment and the model-independent Th/Nb ratios also suggests that the model successfully accounts for the effects of sediment addition to the mantle source region (Fig. 14).

Overall, the calculated amount of sediment addition for Pagan lavas based on the REE melting model verses the Pb and Nd isotopic mixing model agrees well for Mt. Pagan lavas (0.6–1.4% vs. ~0.8–1.9%) and South Pagan lavas (~1.7–1.9% for both models). In contrast, the model results for CVR lavas (0.9–2.1% vs. ~1.9–2.2%) are less consistent. This apparent discrepancy can also be seen in some of the geochemical tracers of sediment addition. For example, CVR lavas generally have lower $^{143}Nd/^{144}Nd$ and Ce/Ce* values, and higher Nb/Zr, Th/Nb, and Pb isotopic ratios than those of South Pagan or Mt. Pagan lavas, which probably reflects a larger amount of sediment in the source of the CVR lavas. In contrast, many CVR lavas have La/Sm ratios that are lower than South Pagan lavas that could suggest a smaller amount of sediment addition to the source region of the CVR. This difference for La/Sm might result from variations in the composition of the subducted sediment. The REE model assumes a single composition of sediment. However, ODP Site 801 sediments are compositionally and mineralogically heterogeneous (Plank and Langmuir 1998). These sediments have a wide range in La/Sm (17–61) and other REE ratios, but much less variable ratios involving HFSE, such as Th/Nb (2.5–3.0). Thus, it is possible that the source of the CVR lavas had a relatively large amount of less LREE-enriched sediment (compared to the source of other Pagan lavas). Based on these observations, the calculated amount sediment addition to Mariana lavas based on the Pb and Nd isotopic mixing

Table 5 Representative results of the REE melting model for Mariana lavas

Sample	SED	DMM	TM-06-243	TM-06-236	TM-06-34	TM-06-202	TM-06-214	TM-06-24	PA-5	PAF3B	AGR5	AGR4B	GUG9	GU21
Description	–	–	CVR	CVR	L-S CVR	SP PRE	SP POST	SP POST	MP POST	MP PRE	Agrigan	Agrigan	Guguan	Guguan
MgO	–	–	5.7	5.6	3.7	5.2	4.9	5.2	5.4	7.3	5.4	4.8	4.2	4.3
La	12.8	0.19	7.41 (0.7)	6.12 (−0.2)	7.45 (0.7)	7.54 (0.9)	8.12 (0.8)	7.63 (1.0)	5.03 (−0.1)	3.49 (−0.1)	7.72 (3.1)	7.72 (2.2)	2.89 (1.5)	3.18 (1.9)
Ce	20.5	0.55	15.4 (0.3)	13.5 (4.4)	15.7 (0.0)	15.9 (−0.7)	17.5 (−0.8)	16.3 (−1.1)	11.2 (2.2)	8.18 (2.5)	15.7 (−1.4)	16.4 (2.4)	7.48 (−1.9)	7.95 (−2.1)
Nd	13.3	0.58	10.3 (−1.9)	8.96 (−4.4)	10.9 (−1.9)	10.9 (−1.6)	11.8 (−1.8)	11.1 (−1.5)	8.42 (−2.4)	6.12 (−2.8)	10.2 (−6.5)	10.2 (−7.7)	6.36 (−3.2)	6.95 (−3.7)
Sm	2.88	0.24	2.94 (−0.5)	2.62 (−3.6)	3.20 (0.1)	3.17 (0.5)	3.45 (1.6)	3.22 (0.6)	2.64 (−3.1)	1.94 (−3.0)	2.86 (0.6)	2.85 (−3.3)	2.20 (3.0)	2.45 (1.2)
Eu	0.75	0.10	0.99 (0.0)	0.98 (0.1)	1.08 (0.0)	0.99 (0.0)	1.05 (0.0)	1.03 (0.0)	0.97 (0.0)	0.73 (0.1)	0.93 (−0.1)	1.04 (0.0)	0.81 (−0.1)	0.88 (0.0)
Gd	2.63	0.36	3.46 (1.0)	3.10 (−1.6)	3.83 (1.3)	3.77 (2.1)	4.10 (1.2)	3.83 (2.2)	3.30 (0.4)	2.41 (2.1)	3.31 (3.5)	3.29 (0.7)	2.90 (1.3)	3.28 (3.4)
Dy	2.38	0.51	3.69 (0.8)	3.29 (−1.5)	4.13 (0.3)	4.04 (0.0)	4.37 (−0.2)	4.10 (1.0)	3.74 (4.1)	2.69 (1.0)	3.48 (5.4)	3.41 (3.2)	3.39 (3.0)	3.96 (3.9)
Er	1.27	0.35	2.20 (0.6)	1.96 (−0.3)	2.47 (0.3)	2.42 (−0.2)	2.60 (0.7)	2.45 (−0.3)	2.29 (1.3)	1.64 (−2.3)	2.06 (0.8)	2.00 (2.7)	2.10 (−0.4)	2.50 (−3.0)
Yb	1.12	0.37	2.09 (0.5)	1.86 (3.7)	2.34 (0.5)	2.30 (0.5)	2.47 (−0.3)	2.33 (−0.6)	2.21 (−0.3)	1.58 (−1.3)	1.94 (−2.3)	1.88 (−0.9)	2.04 (−1.2)	2.46 (−2.7)
Lu	0.17	0.06	0.33 (−1.5)	0.29 (2.5)	0.37 (−1.3)	0.36 (−1.4)	0.39 (−1.3)	0.37 (−1.3)	0.35 (−2.6)	0.25 (3.5)	0.31 (−4.1)	0.30 (−0.3)	0.32 (−2.4)	0.39 (0.3)
Sediment (%)	–	–	2.1	1.3	1.9	1.9	1.7	1.8	1.4	0.9	2.4	1.7	0.4	0.6
Melting (%)	–	–	4.3	2.9	5.5	4.7	4.0	4.4	7.3	5.1	4.2	2.4	9.3	14.6
Oliv/Mt (%)	–	–	+16.3	+9.7	+4.5	+19.5	+20.8	+16.3	−13.2	+18.9	+28.4	+17.0	−3.9	−21.7
Cpx (%)	–	–	−4.4	−2.2	−12.0	−7.2	−8.2	−7.2	−2.4	0.0	−8.9	−6.2	−11.2	−12.3
Plag (%)	–	–	−22.6	−0.7	−21.6	−34.7	−39.2	−31.6	−9.6	−3.5	−25.8	−5.3	−16.1	−18.0
Frac/Accum (%)	–	–	−10.7	+6.8	−29.0	−22.3	−26.6	−22.4	−25.2	+15.4	−6.3	+5.5	−31.2	−52.0
ΣR^2	–	–	9	77	8	11	11	13	46	48	118	100	44	66

Representative model results for the CVR, late-stage CVR (L-S CVR), South Pagan pre-caldera (SP PRE) and post-caldera (SP POST), Mt. Pagan pre-caldera (MP PRE) and post-caldera (MP POST), Agrigan, and Guguan lavas. The compositions for Mt. Pagan, Agrigan, and Guguan lavas are from Woodhead (1989), Elliott et al. (1997), and Stern et al. (2006). The mantle source is assumed to be a mixture of ODP Site 801 sediment and depleted mantle (represented by DMM). The assumed sediment composition (SED) used for the model is an average of three Site 801 stratigraphic units (chert, radiolarite, and volcaniclastic sediment) from Plank and Langmuir (1998). The pelagic clay unit from Site 801 (Plank and Langmuir 1998) was not included because it gave unreasonable model results (i.e., unusually small amounts of sediment, excessive crystal fractionation, and poor ΣR^2 values), which is consistent with the idea that the pelagic clay was scraped off the down going slab as it entered the trench (Wade et al. 2005). The REE abundances of DMM come from Workman and Hart (2005). The compositions of partial melts were calculated using a modal mineralogy of 60% olivine, 20% clinopyroxene, 15% orthopyroxene, and 5% spinel, and the batch melting equation from Shaw (1970). The model could not distinguish between clinopyroxene (Cpx) fractionation and melting of a clinopyroxene-bearing source. Thus, the amount of clinopyroxene fractionation was calculated from the CaO/Al_2O_3 value of each lava (Fig. 3), assuming a parental magma with a CaO/Al_2O_3 value equal to the highest value observed for Pagan lavas (0.7; Woodhead 1989). As discussed in the text, clinopyroxene fractionation is the dominant control on the CaO/Al_2O_3 ratio. The composition of clinopyroxene used for the model is an average of multiple mineral core analyses from Kohut et al. (2006). The amounts of plagioclase, olivine, and magnetite fractionation or accumulation were calculated as described below. Oliv/Mt (%) is the sum of olivine (Oliv) and titanomagnetite (Mt) fractionation and/or accumulation. These two minerals are grouped together in the model because the D values for the REE are assumed to be zero in both minerals. The model melt compositions were allowed to undergo equilibrium crystallization in steps. First, clinopyroxene was removed from the melt (the amount was calculated from CaO/Al_2O_3 as described earlier). Second, the residual melt was allowed to undergo equilibrium fractionation or accumulation of plagioclase (Plag) followed by olivine/titanomagnetite. An incorrect amount of plagioclase fractionation and accumulation does not have a significant effect on the model source or melting parameters because the mineral/melt partition coefficients for the REE are all relatively small in plagioclase, excluding Eu (Table 4). In practice, the amount of plagioclase fractionation or accumulation calculated in the model is proportional to the size of the Eu anomaly. The model parameters (mantle-sediment mixing proportions, degree of partial melting of the mixed source, and the amount of olivine/titanomagnetite and plagioclase fractionation or accumulation were varied to minimize the sum of the residuals squared (ΣR^2 value) on the REE abundances for each sample. Model results for lavas that fractionated or accumulated minerals are noted by negative and plus signs, respectively. For comparison, the expected ΣR^2 equals ~ 123 ($\pm 2\sigma$) based on the analytical uncertainty of the REE data. The model results for each sample are given with the residuals (% difference) on the concentration of each REE shown in parentheses as $100 \times$ [(calculated abundance/observed abundance) − 1]. Frac/accum (%) is the sum of olivine/titanomagnetite, clinopyroxene, and plagioclase fractionation and/or accumulation for the model results of each sample. Four REE (Pr, Tb, Ho, and Tm) are excluded from the model because Site 801 sediment was not analyzed for these elements. Evolved Mariana lavas with <3.5 wt. % MgO were not modeled. The mineral/melt partition coefficients used for the model calculations are shown in Table 4. Results for all of the modeled Pagan, Guguan, and Agrigan samples are presented in Table A2—Electronic Supplementary Material

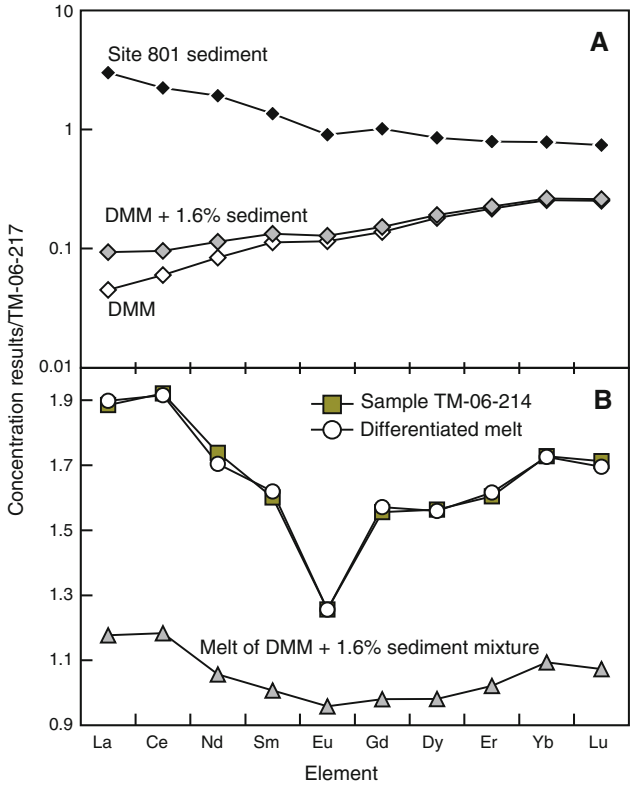

Fig. 12 Mass-balance REE melting model results for a representative South Pagan sample, TM-06-214. An explanation of the model calculations and parameters is given in Table 5. All REE patterns are normalized to a relatively mafic CVR sample (TM-06-217). **a** The REE profiles for depleted MORB mantle (DMM; *white diamonds*), ODP Site 801 sediment (*black diamonds*), and the calculated mixture of the two sources (DMM + 1.6% sediment; *gray diamonds*). **b** Partial melting of the DMM + 1.6% sediment source (*triangles*) and subsequent crystal fractionation (*open circles*) produces a saucer-shaped REE pattern that closely matches the REE profile of sample TM-06-214 (*squares*)

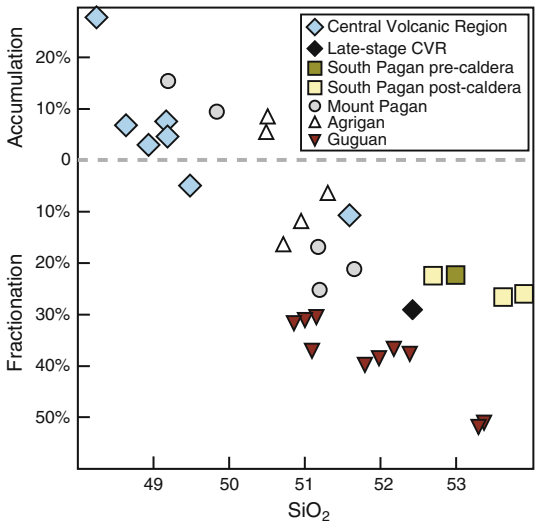

Fig. 13 SiO_2 versus the calculated amount of crystal fractionation or accumulation for Mariana lavas. The amount of crystallization or accumulation (in %) was calculated using the REE melting model presented in Table 5. Data sources for Mariana lavas are given in the caption to Fig. 6. The *symbols* are defined in the *key*. The 2σ *error bar* for SiO_2 is smaller than the size of the *symbols*

Table 6 Summary of REE melting model results

Location	Sediment	Melting	Fluid content
Agrigan	1.6–2.4% (2.0%)	2.4–4.7% (3.5%)	Low
Mt. Pagan	0.6–1.4% (0.9%)	4.1–7.3% (5.0%)	High
CVR	0.9–2.1% (1.4%)	3.0–4.3% (3.6%)	Low
South Pagan	1.7–1.9% (1.8%)	4.0–4.7% (4.3%)	Low
Guguan	0.3–0.9% (0.6%)	9.0–14.6% (11.0%)	High

The ranges in amount of sediment and degree of partial melting calculated for Mariana lavas are shown (average values in parentheses). The late-stage CVR lavas are excluded. The relative amount of fluid addition is estimated from the Ba/Th ratios of the lavas. The volcanoes are listed by location from north to south

model is thought to be more accurate than the REE model estimates.

The calculated degree of partial melting based on the REE melting model for Pagan (3–7%), Agrigan (2–5%), and Guguan (9–15%) lavas is similar to or lower than previous estimates for Mariana lavas (6–30%; Bloomer et al. 1989b; Peate and Pearce 1998; Turner et al. 2006). The melt fractions (Table 6) required to match the REE abundances of the CVR lavas (3.0–4.3%, excluding a late-stage lava with 5.5%) and South Pagan lavas (4.0–4.7%) are generally lower than those from Mt. Pagan lavas (4.0–7.3%). Some REE ratios (e.g., Sm/Yb and La/Yb) have been used to decipher melting variations within the subarc mantle (e.g., Asimow and Langmuir 2003; Kelemen et al. 2003; Stern et al. 2006). As expected, the calculated degree of partial melting from the REE melting model correlates with the Sm/Yb ratios of Mariana lavas. Although this relationship is model dependant, this correlation illustrates the idea that the melt fraction, rather than the amount of sediment addition, is the dominant control on the MREE/HREE ratios of Mariana lavas. In addition, the model-independent Ba/Th and Ba/La (not shown) ratios broadly correlate with the calculated degree of partial melting (Fig. 14). In detail, Guguan lavas have the highest Ba/Th and Ba/La ratios and lowest Sm/Yb ratios among Mariana lavas (Figs. 6a, 14), which is consistent with a relatively large fluid contribution and high degree of partial melting (and vise versa for South Pagan, CVR, and Agrigan lavas). Mount Pagan lavas are intermediate (Fig. 14). These observations suggest that the fluid flux to the subarc mantle may be the dominant control on the extent of partial melting for Mariana arc volcanoes (Kelley et al. 2010). Similar correlations between the amount of fluid supplied to the mantle wedge and the

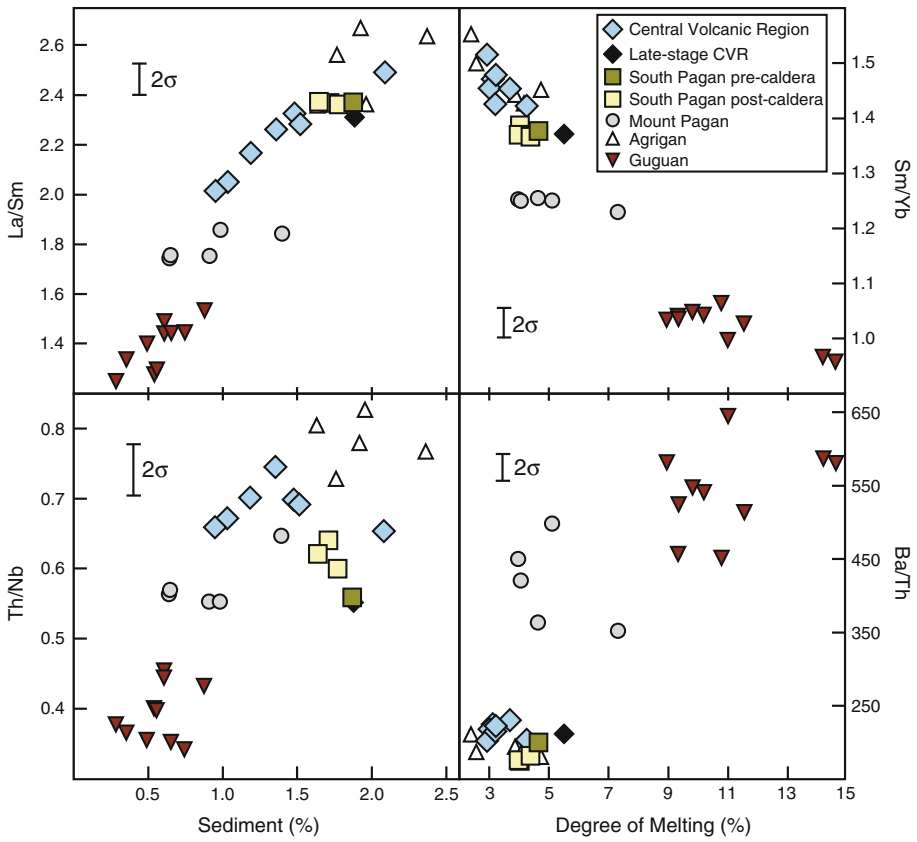

Fig. 14 Incompatible trace element ratios versus the calculated amount of sediment addition to the mantle source and the degree of partial melting for Mariana lavas. The model parameters were calculated using the REE melting model presented in Table 5. Data sources for the Mariana lavas are given in the caption to Fig. 6. The *symbols* are defined in the *key*. The 2σ *error bars* for the trace element ratios are shown on each *panel*

degree of partial melting have also been recognized along other arc fronts (Ishizuka et al. 2007; Portnyagin et al. 2007; Rychert et al. 2008).

Dynamics of the partial melting process beneath Pagan Island

Geochemical variations of cross-arc volcanoes (oriented perpendicular to the strike of the magmatic front) provide a unique constraint on the nature of the mantle source and melting conditions within arc systems (Gill 1981; Ryan et al. 1996; Stern et al. 2006). Cross-arc variations in lava chemistry were observed for Guguan volcanoes separated by 8–29 km (Stern et al. 2006). South Pagan caldera lies ~6 km further west than Mt. Pagan caldera (Fig. 2) and it is located slightly west of the main arc axis defined by active Mariana volcanoes (dashed line on Fig. 1). This ~6-km offset is only slightly smaller than the low end of the range for Guguan volcanoes. Based on the seismic profile of the Wadati Benioff Zone below the central portion of the Mariana arc in Engdahl et al. (1998), this ~6-km horizontal distance would translate to a ~20 km greater depth to the slab beneath South Pagan. This might be large enough to allow for cross-arc variations in the melting and source processes on the scale of the distance between these volcanoes. In this case, the lower Ba/Th and $^{143}Nd/^{144}Nd$, and higher Nb/Zr, La/Sm, Sm/Yb, and Pb isotopic ratios at South Pagan compared to Mt. Pagan might result from cross-arc geochemical variations characterized by a westward decrease in the fluid contribution and melt fraction, and/or an increase in the mass fraction of sediment melted with increasing distance and depth from the trench (e.g., Stern et al. 2006). However, it is also possible these geochemical differences reflect along-arc variations in the sediment- and fluid-modified mantle source composition, although no clear systematic spatial variations of incompatible trace element or isotopic ratios are observed for Agrigan, Pagan, and Guguan.

The range in the amount of sediment addition to the source of Mt. Pagan lavas (~0.8–1.9%) is an order of magnitude greater than the range for South Pagan lavas (~1.8–1.9%). In detail, the $^{206}Pb/^{204}Pb$ and $^{143}Nd/^{144}Nd$ variability in Mt. Pagan lavas is equivalent to 64 and 45% of the total range observed in Mariana lavas (Fig. 8). There is considerably less variation in the $^{206}Pb/^{204}Pb$ and $^{143}Nd/^{144}Nd$ ratios of South Pagan lavas (2 and 12%, respectively). These observations can be potentially explained if greater extents of partial melting in the source region of Mt. Pagan (compared to South Pagan) facilitated the extraction of melt from a wider region. Partial melting over a larger area is more likely to sample a greater range in the amount of subducted sediment. Overall, the

differences in the amount of fluid and sediment within the source regions of these neighboring volcanoes (Table 6), and the short-term compositional variations at Mt. Pagan (Fig. 9b) and South Pagan (Fig. 7) suggest that the length scale of compositional heterogeneity in the mantle wedge is small with respect to the distance between the summits of these volcanoes (~10 km).

Conclusions

The geochemical variability of Pagan Island lavas provides an excellent opportunity to examine the mantle source (i.e., slab components) and melting dynamics within the Mariana intra-oceanic arc. Two main eruptive sequences, the pre-caldera (780–9.4 ka) and post-caldera (<9.4 ka) stages, have been recognized for South Pagan. The eruptive history of the extinct Quaternary CVR is poorly constrained, although stratigraphic relationships and $^{40}Ar/^{39}Ar$ dating indicate that the CVR is older than the South Pagan pre-caldera stage. Olivine, clinopyroxene, titanomagnetite, and plagioclase fractionation, plagioclase accumulation, and magma mixing are important crustal processes for these lavas. Despite their proximity to Mt. Pagan, CVR and South Pagan volcanoes have erupted mostly geochemically distinct lavas reflecting variations in slab contributions (i.e., sediment and aqueous fluid) to the mantle wedge and the extent of mantle partial melting. Lead and Nd isotopic mixing calculations indicate the average sediment contribution to CVR (~2.1%), Agrigan (~2.0%), and South Pagan (~1.8%) lavas is slightly higher than Mt. Pagan (~1.4%) and Guguan (~1.3%) lavas. Melt modeling demonstrates that saucer-shaped normalized REE patterns observed in Pagan lavas can arise from partial melting of a mixed mantle-sediment source and do not require amphibole interaction or fractionation to depress the middle REE abundances of the lavas. The modeled degree of mantle partial melting based on the REE melting model for Agrigan (2–5%), Pagan (3–7%), and Guguan (9–15%) lavas correlates with indicators of fluid addition (e.g., Ba/Th), which suggests that the fluid flux to the mantle wedge is the dominant control on the extent of partial melting beneath Mariana arc volcanoes. An increase in the sediment contribution (higher Th/Nb, La/Sm, and Pb isotopic ratios), and decrease in the amount of fluid addition (lower Ba/Th) and extent of melting (higher Sm/Yb) from Mt. Pagan to South Pagan could reflect systematic cross-arc or irregular along-arc melting variations. These observations indicate that the length scale of compositional heterogeneity in the mantle wedge is small with respect to the distance between the summits of these volcanoes (~10 km).

Acknowledgments We would like to thank Julie Herring, Game McGimsey, Maurice Sako, and Daisy Wheeler for assistance during the Pagan fieldwork. Our warmest aloha to Mike Cunningham of Americopters, the CNMI Emergency management office personnel (especially Juan Camacho, Ramon Chong, and Joe Kaipat), the crew of the Tenshe 2, and the Pagan residents for helping with the island transportation, field logistics, and hunting our food. Much appreciation goes to Joan Willis for her assistance in the clean laboratory at SDSU. We thank Jim Gill, John Pallister, Ian Ridley and an anonymous reviewer for their critical and helpful reviews. This research was funded by the United States Geological Survey to F.A.T., National Science Foundation grants to M.O.G. (EAR 07-38817) and A.J.P. (EAR 07-38671), and two Harold T. Stearns Fellowship grants awarded to J.P.M. This is SOEST contribution number 7573.

References

Arculus RJ, Johnson RW (1981) Island arc magma sources: a geochemical assessment of the roles of slab-derived components and crustal contamination. Geochem J 15:109–133

Asimow PD, Langmuir CH (2003) The importance of water to oceanic mantle melting regimes. Nature 421:815–820

Ayers JC, Dittmer SK, Layne GD (1997) Partitioning of elements between peridotite and H_2O at 2.0–3.0 GPa and 900–1100°C and application to models of subduction zone processes. Earth Planet Sci Lett 150:381–398

Bach W, Hegner E, Erzinger J, Satir M (1994) Chemical and isotopic variations along the superfast spreading East Pacific Rise from 6 to 30°S. Contrib Mineral Petrol 116:365–380

Banks NG, Koyanagi RY, Sinton JM, Honma KT (1984) The eruption of Mount Pagan volcano, Mariana Islands, 15 May 1981. J Volcanol Geotherm Res 22:225–269

Bloomer SH, Stern RJ, Smoot NC (1989a) Physical volcanology of the submarine Mariana and volcano arcs. Bull Volcanol 51:210–224

Bloomer SH, Stern RJ, Fisk E, Geschwind CH (1989b) Shoshonitic volcanism in the Northern Mariana Arc 1. Mineralogic and major and trace element characteristics. J Geotherm Res 94:4469–4496

Bolge LL, Carr MJ, Feigenson MD, Alvarado GE (2006) Geochemical stratigraphy and magmatic evolution at Arenal volcano, Costa Rica. J Volcanol Geotherm Res 157:34–48

Brenan JM, Shaw HF, Ryerson FJ, Phinney DL (1995) Mineral-aqueous fluid partitioning of trace elements at 900°C and 2.0 GPa: constraints on the trace element chemistry of mantle and deep crustal fluids. Geochim Cosmochim Acta 59:3331–3350

Chauvel C, Blichert-Toft J (2001) A hafnium isotope and trace element perspective on melting of the depleted mantle. Earth Planet Sci Lett 190:137–151

Class C, Miller DM, Goldstein SL, Langmuir CH (2000) Distinguishing melt and fluid subduction components in Umnak Volcanics, Aleutian Arc. Geochem Geophys Geosyst 1. doi: 10.1029/1999GC000010

Corwin G, Bonham LD, Terman MJ, Viele GW (1957) Military geology of Pagan, Mariana Islands: U.S. Army Corps of Engineers, Intelligence Dossier, p 259

Davidson J, Turner S, Handley H, Macpherson C, Dosseto A (2007) Amphibole "sponge" in arc crust? Geology 35:787–790

Dixon TH, Batiza R (1979) Petrology and geochemistry of recent lavas in the Northern Marianas. Contrib Mineral Petrol 70:167–181

Dufrane SA, Turner S, Dosseto A, van Soest M (2009) Reappraisal of fluid and sediment contributions to Lesser Antilles magmas. Chem Geol 265:272–278

Dungan MA, Wulff A, Thompson R (2001) Eruptive stratigraphy of the Tatara-San Pedro Complex, 36°S, Southern Volcanic Zone, Chilean Andes: reconstruction method and implications for magma evolution at long-lived arc volcanic centers. J Petrol 42:555–626

Elburg M, Foden J (1998) Temporal changes in arc magma geochemistry, northern Sulawesi, Indonesia. Earth Planet Sci Lett 163:381–398

Elliott T, Plank T, Zindler A, White W, Bourdon B (1997) Element transport from slab to volcanic front at the Mariana arc. J Geophys Res 102(B7):14991–15019

Engdahl ER, van der Hilst RD, Buland R (1998) Global teleseismic earthquake relocation with improved travel times and procedures for depth determination. Bull Seismol Soc Am 88:722–743

Figueroa O, Deruelle B, Demaiffe D (2009) Genesis of adakite-like lavas of Licancabur volcano (Chile-Bolivia, Central Andes). Comptes Rendus Geosci 341:310–318

Galer SJG, Abouchami W (1998) Practical application of lead triple spiking for correction of instrumental mass discrimination. Min Mag 62A:491–492

George R, Turner S, Hawkesworth C, Morris J, Nye C, Ryan J, Zheng S-H (2003) Melting processes and fluid and sediment transport rates along the Alaska-Aleutian arc from an integrated U–Th–Ra–Be isotope study. J Geophys Res 108(B5). doi:10.1029/2002JB001916

Gill JB (1981) Orogenic andesite and plate tectonics. Springer, Berlin, p 390

Hart SR (1984) A large scale isotope anomaly in the Southern Hemisphere mantle. Nature 309:753–757

Hawkesworth CJ, Hergt JM, Ellam RM, McDermott F (1991) Element fluxes associated with subduction related magmatism. Philos Trans R Soc Lond A 335:393–405

Hochstaedter A, Gill J, Peters R, Broughton P, Holden P (2001) Across-arc geochemical trends in the Izu-Bonin arc: contributions from the subducting slab. Geochem Geophys Geosyst 2. doi:10.1029/2008GC000105

Hofmann AW (1988) Chemical differentiation of the Earth: the relationship between mantle, continental crust, and oceanic crust. Earth Planet Sci Lett 90:297–314

Ishizuka O, Taylor RN, Yuasa M, Milton JA, Nesbitt RW, Uto K, Sakamoto I (2007) Processes controlling along-arc isotopic variation of the southern Izu-Bonin arc. Geochem Geophys Geosyst 8. doi:10.1029/2006GC001475

Jicha BR, Singer BS, Brophy JG, Fournelle JH, Johnson CM, Beard BL, Lapen TJ, Mahlen NJ (2004) Variable impact of the subducted slab on Aleutian Island arc magma sources: evidence from Sr, Nd, Pb, and Hf isotopes and trace element abundances. J Petrol 45:1845–1875

Jicha BR, Hart GL, Johnson CM, Hildreth W, Beard BL, Shirey SB, Valley JW (2009) Isotopic and trace element constraints on the petrogenesis of lavas from the Mount Adams volcanic field, Washington. Contrib Mineral Petrol 157:189–207

Johnson MC, Plank T (1999) Dehydration and melting experiments constrain the fate of subducted sediments. Geochem Geophys Geosyst 1. doi:10.1029/1999GC000014

Johnson DM, Hooper PR, Conrey RM (1999) XRF analysis of rocks and minerals for major and trace elements on a single low dilution Li-tetraborate fused bead. Adv X-ray Anal 41:843–867

Jolly WT, Lidiak EG, Dickin AP, Way T-W (2002) Recycling in the Puerto Rican mantle wedge, Greater Antilles island arc. The Island Arc 11:10–24

Karig DE (1971) Structural history of the Mariana Island Arc system. Geol Soc Am Bull 82:323–344

Kelemen PB, Yogodzinski GM, Scholl DW (2003) Along-strike variations in the Aleutian island arc: genesis of high Mg# andesite and implications for continental crust. Tracers of the slab. In: Eiler J (ed) Inside the subduction factory, vol 138. American Geophysical Union, Geophysical Monograph, Washington, DC, pp 223–276

Kelley KA, Plank T, Newman S, Stolper EM, Grove TL, Parman S, Hauri EH (2010) Mantle melting as a function of water content beneath the Mariana arc. J Petrol 51:1711–1738

Kent AJR, Elliott TR (2002) Melt inclusions from Marianas arc lavas: implications for the composition and formation of island arc magmas. Chem Geol 183:263–286

Keppler H (1996) Constraints from partitioning experiments on the composition of subduction-zone fluids. Nature 380:237–240

Kessel R, Schmidt MW, Ulmer P, Pettke T (2005) Trace element signature of subduction-zone fluids, melts and supercritical liquids at 120–180 km depth. Nature 437:724–727

Knaack C, Cornelius SB, Hooper PR (1994) Trace element analyses of rocks and minerals by ICP-MS. Open file report, GeoAnalytical Lab, Washington State University

Kohut EJ, Stern RJ, Kent AJR, Nielsen RL, Bloomer SH, Matthew L (2006) Evidence for adiabatic decompression melting in the southern Mariana arc from high-Mg lavas and melt inclusions. Contrib Mineral Petrol 152:201–221

Larocque J, Canil D (2010) The role of amphibole in the evolution of arc magmas and crust: the case from the Jurassic Bonanza arc section, Vancouver Island, Canada. Contrib Mineral Petrol 159:475–492

Larson EE, Reynolds R, Merrill R, Levi S, Ozima M, Aoki Y, Kinoshita H, Zasshu S, Kawai N, Nakajima T, Hirooka D (1974) Major-element petrochemistry of some extrusive rocks from the volcanically active Mariana Islands. Bull Volcanol 38:361–377

Macpherson CG, Dreher ST, Thirlwall MF (2006) Adakites without slab melting: high pressure differentiation of island arc magma, Mindanao, the Philippines. Earth Planet Sci Lett 243:581–593

Mahoney JJ, Sinton JM, Kurz MD, Macdougall JD, Spencer KJ, Lugmair GW (1994) Isotope and trace element characteristics of a super-fast spreading ridge: East Pacific Rise, 13–23°S. Earth Planet Sci Lett 121:173–193

Marchesi C, Garrido CJ, Bosch D, Proenza JA, Gervilla F, Monie P, Rodriguez-Vega A (2007) Geochemistry of Cretaceous magmatism in eastern Cuba: recycling of North American continental sediments and implications for subduction polarity in the Greater Antilles paleo-arc. J Petrol 48:1813–1840

Marske JP, Pietruszka AJ, Weis D, Garcia MO, Rhodes JM (2007) Rapid passage of a small-scale heterogeneity through the melting regions of Kilauea and Mauna Loa volcanoes, Hawaii. Earth Planet Sci Lett 259:34–50

Meijer A (1976) Pb and Sr isotopic data bearing on the origin of volcanic rocks from the Mariana island-arc system. Geol Soc Am Bull 87:45–51

Meijer A, Reagan M (1981) Petrology and geochemistry of the island of Sarigan in the Mariana Arc: calc-alkaline volcanism in an oceanic setting. Contrib Mineral Petrol 77:337–354

Naumann TR, Geist DJ (1999) Generation of alkali-olivine basalts by fractionation of tholeiitic magma. Geology 27:423–426

Nielsen RL (1992) BIGD: a FORTRAN program to calculate trace-element partition coefficients for natural mafic and intermediate composition magmas. Comp Geosci 18:773–788

Nielsen RL, Gallahan WE, Newberger F (1992) Experimentally determined mineral-melt partition coefficients for Sc, Y and REE for olivine, orthopyroxene, pigeonite, magnetite and ilmenite. Contrib Mineral Petrol 110:488–499

Peate DW, Pearce JA (1998) Causes of spatial compositional variations in Mariana arc lavas: trace element evidence. The Island Arc 7:479–495

Phinney WC, Morrison DA (1990) Partition coefficients of calcic plagioclase: implications for Archean anorthosites. Geochim Cosmochim Acta 54:1639–1654

Pietruszka AP, Garcia MO (1999) A rapid fluctuation in the mantle source and melting history of Kilauea volcano inferred from the geochemistry of its historical summit lavas (1790–1982). J Petrol 40:1321–1342

Plank T, Langmuir C (1998) The chemical composition of subducting sediment and its consequence for the crust and mantle. Chem Geol 145:325–394

Portnyagin M, Hoernle K, Plechov P, Mironov N, Khubunaya S (2007) Constraints on mantle melting and composition, and nature of slab components in volcanic arcs from volatiles (H2O, S, Cl, F) and trace elements in melt inclusions from the Kamchatka Arc. Earth Planet Sci Lett 255:53–69

Rhodes JM, Vollinger MJ (2004) Composition of basaltic lavas sampled by phase-2 of the Hawaii Scientific Drilling Project: geochemical stratigraphy and magma types. Geochem Geophys Geosyst 5. doi:10.1029/2004GC000895

Ryan JG, Morris J, Bebout G, Leeman WP (1996) Describing chemical fluxes in subduction zones: insights from "depth profiling" studies of arc and forearc rocks. In: Bebout G (ed) Subduction: top to bottom, vol 96. American Geophysical Union, Geophysical Monograph, Washington DC, pp 263–268

Rychert CA, Fischer, KM, Abers, GA, Plank T, Syracuse E, Protti JM, Gonzalez V, Strauch W (2008) Strong along-arc variations in attenuation in the mantle wedge beneath Costa Rica and Nicaragua. Geochem Geophys Geosyst 9. doi:10.1029/2008GC002040

Salters VJM, Longhi J (1999) Trace element partitioning during the initial stages of melting beneath mid-ocean ridges. Earth Planet Sci Lett 166:15–30

Shaw DM (1970) Trace element fractionation during anatexis. Geochim Cosmochim Acta 34:237–243

Shaw AM, Hauri EH, Fischer TP, Hilton DR, Kelley KA (2008) Hydrogen isotopes in Mariana arc melt inclusions: implications for subduction dehydration and the deep-Earth water cycle. Earth Planet Sci Lett 275:138–145

Simkin T, Siebert L, McClelland L, Bridge D, Newhall C, Latter JH (1981) Volcanoes of the World. Smithson Inst, Stroudsburg, p 232

Singer BS, Relle MR, Hoffman KA, Battle A, Guillou H, Laj C, Carracedo JC (2002) Ar/Ar ages of transitionally magnetized lavas on La Palma, Canary Islands, and the geomagnetic instability timescale. J Geophys Res 107(B11). doi:10.1029/2001JB001613

Sisson TW (1994) Hornblende-melt trace-element partitioning measured by ion microprobe. Chem Geol 117:331–344

Stern CR, Kilian R (1996) Role of the subducted slab, mantle wedge and continental crust in the generation of adakites from the Andean Austral Volcanic Zone. Contrib Mineral Petrol 123:263–281

Stern RJ, Fouch MJ, Klemperer S (2003) An overview of the Izu-Bonin-Mariana subduction factory. In: Eiler J, Hirschmann M (eds) Inside the subduction factory, vol 138. AGU Monograph, Washington DC, pp 175–222

Stern RJ, Kohut E, Bloomer SH, Leybourne M, Fouch M, Vervoort J (2006) Subduction factory processes beneath the Guguan cross-chain, Mariana Arc: no role for sediments, are serpentinites important? Contrib Mineral Petrol 151:202–221

Sun SS, McDonough WF (1989) Chemical and isotopic systematics of oceanic basalts: implications for mantle composition and processes. In: Saunders AD, Norry MJ (eds) Magmatism in the ocean basins. Geol Soc Lon Spec Pub 42:315–345

Thirlwall MF (2002) Multicollector ICP-MS analysis of Pb isotopes using a ^{207}Pb–^{204}Pb double spike demonstrates up to 400 ppm/amu systematic errors in Tl-normalization. Chem Geol 184:255–274

Tollstrup DL, Gill JB (2005) Hafnium systematics of the Mariana arc: evidence for sediment melt and residual phases. Geology 33:737–740

Trusdell FA (2009) Geology of the Mariana Islands. In: Gillespie RG, Clague DA (eds) Encyclopedia of Islands: Encyclopedias of the Natural World. University of California press, California, pp 598–603

Trusdell FA, Moore RB, Sako MK (2006) Preliminary geologic map of Mount Pagan Volcano, Pagan Island, Commonwealth of the Northern Mariana Islands: U.S. Geol Survey Open-File Report 2006-1386, p 32

Turner SP, Hawkesworth CJ (1997) Constraints on flux rates and mantle dynamics beneath island arcs from Tonga-Kermadec lava geochemistry. Nature 389:568–573

Turner SP, Regelous M, Hawkesworth CJ, Rostami K (2006) Partial melting processes above subducting plates: constraints from ^{231}Pa–^{235}U disequilibria. Geochim Cosmochim Acta 70:480–503

Vlastevic I, Aslanian DLD, Bougault H, Olivet JL, Geli L (1999) Large-scale chemical and thermal division of the Pacific mantle. Nature 399:345–350

Wade JA, Plank T, Stern RJ, Tollstrup DL, Gill JB, O'Leary JC, Eiler JM, Moore RB, Woodhead JD, Trusdell F, Fischer TP, Hilton DR (2005) The May 2003 eruption of Anatahan volcano, Mariana Islands: geochemical evolution of a silicic island-arc volcano. J Volcanol Geotherm Res 146:139–170

Wendt JI, Regelous M, Niu Y, Hekinian R, Collerson KD (1999) Geochemistry of lavas from the Garrett Transform Fault: insights into mantle heterogeneity beneath the eastern Pacific. Earth Planet Sci Lett 173:271–284

Woodhead JD (1989) Geochemistry of the Mariana arc (western Pacific): source compositions and processes. Chem Geol 76:1–24

Workman RK, Hart SR (2005) Major and trace element composition of the depleted MORB mantle (DMM). Earth Planet Sci Lett 231:53–72

Yokoyama T, Kobayashi K, Kuritani T, Nakamura E (2003) Mantle metasomatism and rapid ascent of slab components beneath island arcs: evidence from ^{238}U–^{230}Th–^{226}Ra disequilibria of Miyakejima volcano, Izu arc, Japan